

# 1 Marine Heatwaves in the Arabian Sea

2 Abhisek Chatterjee<sup>1</sup>, Gouri Anil<sup>1,2</sup>, Lakshmi R Shenoy<sup>1,3</sup>

3 <sup>1</sup>Indian National Centre for Ocean Information Services, Ministry of Earth Sciences, Hyderabad, India

4 <sup>2</sup>Cochin University of Science and Technology, Cochin, India

5 <sup>3</sup>Kerala University of Fisheries and Ocean Studies, Cochin, India

6 *Correspondence to:* Abhisek Chatterjee ([abhisek.c@incois.gov.in](mailto:abhisek.c@incois.gov.in))

7

8 **Abstract.** Marine heatwaves (MHWs) are prolonged warm sea condition events that can cause a destructive impact on marine  
9 ecosystems. The documentation of MHWs and assessment of their impacts is largely confined to a few regional seas or in  
10 global mean studies. The north Indian Ocean received almost no attention in this regard despite the fact that this ocean basin,  
11 particularly the Arabian Sea, is warming at the most rapid pace among the other tropical basins in recent decades. This study  
12 shows the characteristics of MHW events for the Arabian Sea during 1982-2019. Our analysis shows that the duration  
13 (frequency) of MHWs exhibits a rapidly increasing trend of ~20 days/decade (1.5-2 count/decade) in the northern Arabian Sea  
14 and the southeastern Arabian Sea close to the west coast of India; which is a multi-fold increase in the MHW days (frequency)  
15 from the 80s'. Notably, since the beginning of the satellite record, the years 2010 and 2016 exhibit the maximum number of  
16 heatwave days when more than 75% of days of the pre-monsoon and summer-monsoon season experience heatwaves. The  
17 accelerated trend of the heatwave days is found to be driven by the rapid rise of the mean SST of the Arabian Sea in the recent  
18 decade. Moreover, longer heatwave days are also associated with the dominant climate modes. Among them, the Indian Ocean  
19 Basin mode via the decaying phase of the El-Niño is the most influencing mode contributing to more than 70-80% of observed  
20 heatwave days in this basin. Further analysis of the most prolonged observed heatwave during April-June 2010 indicates that  
21 surface heat flux associated with the weaker latent heat loss and the shallow mixed layer was the primary cause of this event.  
22 Further, we note that the pre-monsoon cyclonic storms in the Arabian Sea often contribute to the waning of such heatwaves in  
23 the basin.

## 24 1 Introduction

25 Sea surface temperature (SST) shows significant variability over a large spectrum of frequencies in space and time across the  
26 globe. However, there are times when extremes of such variability occur, causing severe stress to the local ecosystem and  
27 economies driven by such ecosystems. These warmer than normal extreme ocean conditions are referred to as Marine  
28 Heatwaves (MHWs) and are defined as prolonged anomalously warm ocean conditions exceeding a pre-defined threshold  
29 (Pearce et al., 2011; Hobday et al., 2016). The term "Marine Heatwave" was first coined to describe the Ningaloo Niño off the  
30 western coast of Australia during spring 2011 (Feng et al., 2013). These extreme warm events are shown to be responsible for

31 widespread coral bleaching (Feng et al., 2013; Hughes et al., 2017), loss of Kelp forest off the coast of Australia and New  
32 Zealand (Wernberg et al., 2016; Thomsen et al., 2019), reduction in seagrass meadows (Arias et al., 2018) and widespread  
33 harmful algal blooms (Trainer et al., 2020). Further, these events have also been shown to impact economically important  
34 fishery industries in the northwest Atlantic (Mills et al., 2013), northeast Pacific (Cavole et al., 2016) and coastal Australia  
35 (Caputi et al., 2016). Owing to their devastating nature, MHWs and their generating mechanisms received a lot of attention in  
36 the recent decade. Studies of major MHWs that appeared in various parts of the world over the last decade suggest that  
37 evolution and the forcing mechanisms of such events differ considerably from region to region and predominantly depend on  
38 the local air-sea coupling, atmospheric conditions, oceanic preconditions and remote climatic teleconnections (Holbrook et al.,  
39 2019; Oliver et al., 2021). For example, persistent large scale positive atmospheric pressure anomaly ridge caused  
40 unprecedented warm SST in the northeastern Pacific during 2013-2016 with anomalies exceeding more than 3°C (Bond et al.,  
41 2015; Lorenzo and Mantua, 2016). A similar mechanism was at play during the summer of 2003 in the Mediterranean Sea  
42 (Olita et al., 2006) and in the Tasman Sea during the summer of 2017/18 off the coast of New Zealand (Salinger et al., 2019).  
43 On the other hand, advection of warm water was found to be a major driver for the widespread MHW along the western coast  
44 of Australia in 2011 (Feng et al., 2013), in the tropical ocean around Australia in 2015/2016 (Benthuisen et al., 2018), southeast  
45 of Australia in the Tasman Sea during 2015/16 (Oliver et al., 2017) and off the coast of California (Durazo et al., 2002).  
46 Climate variabilities also play a significant role in modulating MHWs in the tropical/extratropical oceans (Holbrook et al.,  
47 2019). Among them, El-Niño Southern Oscillation (ENSO) is shown to be the dominant climate mode that influences MHW  
48 occurrence and duration in the tropical Pacific (Holbrook et al., 2020). In the Indian Ocean, the positive phase of ENSO (Roxy  
49 et al., 2014; Chakravorty et al., 2014; Swapna et al., 2014), Indian Ocean Basin Mode (Klein et al., 1999; Du et al., 2009) and  
50 Indian Ocean Dipole mode (Saji et al., 1999; Chowdary and Gnanaseelan, 2007) favour warming of SST in large part of the  
51 basin. In the extratropics, in the interannual time scale, MHWs in the northeast Pacific is primarily associated with the positive  
52 phase of Pacific Decadal Oscillation (PDO). However, in the longer time scale, the Pacific Decadal Oscillation and North  
53 Pacific Gyre Oscillation (NGPO) contributes to the genesis of heatwaves (Lorenzo and Mantua, 2016). On the other hand, the  
54 North Atlantic Oscillation (NAO) shows strong associations in the MHWs of the northwest Atlantic (Scannell et al., 2016).

55  
56 Notably, over the last few decades, the Indian Ocean, particularly the Arabian Sea, has seen rapid warming at a rate much  
57 faster than the other tropical basins (Levitus et al., 2012). This warming not only shows a negative influence on the primary  
58 productivity of the Arabian Sea (Roxy et al., 2016) but also influences a shift in the phytoplankton community from diatoms  
59 to *Noctiluca scintillans* in the northern Arabian Sea (Goes et al., 2020), reduced rainfall in the Indian continent (Roxy et al.,  
60 2015) and increase flood in the Indian mainland (Ajaymohon and Suryachandra, 2008). Moreover, the frequency of  
61 cyclogenesis in the Arabian Sea has increased over the last few decades, primarily believed to be driven by this rapid rise in  
62 the SST (Murakami et al., 2020; Deshpande et al., 2021). However, the impact of persistent MHW on this enhanced  
63 cyclogenesis is still yet to be explored. While the understanding of the genesis of MHWs across the globe advanced rapidly  
64 over the last decade, there are not many studies to document these events in the northern Indian Ocean. In a recent study,

65 Saranya et al. (2022) discussed the genesis of MHWs in the western Arabian Sea and in the northern Bay of Bengal during  
66 summer and their connection to the Indian summer monsoon.

67

68 Further, the southeastern Arabian Sea and the northern Arabian Sea are economically very important as they constitute one of  
69 the major fishing zones in the Arabian Sea. As per the recent report from Central Marine Fisheries Research Institute, India  
70 (CMFRI, 2007), total fish landing from the Indian exclusive economic zones (EEZ) is  $2.49 \times 10^6$  tonnes during 2001-2005,  
71 and among them, 67% of the catch is from the eastern Arabian Sea (Shankar et al., 2018). Hence, like other parts of the global  
72 ocean, MHWs in this region are very likely significantly influencing the local marine ecosystem, the migration of species and  
73 the associated fishery-dependent economy. Therefore, documenting and understanding the genesis of MHWs in the Arabian  
74 Sea, particularly in the coastal oceans that possess significant economic importance, is necessary for better predicting these  
75 MHWs and assessing their impacts on this region. Hence, in this study, we document MHWs in the Arabian Sea with a  
76 particular emphasis on the coastal waters close to the west coast of India and try to decipher the possible physical mechanisms  
77 that influence the genesis of such heatwaves in this region. Next, Section 2 describes the data we use and the model  
78 configuration, experiments, and forcing. The observed trends in the MHWs are discussed in Section 3. The influence of the  
79 SST trend and the variabilities are given in Section 4. In Section 5, the impact of various climate modes is discussed. In Section  
80 6, the role of different physical processes for the heatwaves during 2010 is presented as a case study. Finally, Section 7  
81 summarises our main results and discusses the possible implications of this study.

## 82 **2 Data and Methodology**

### 83 **2.1 Sea Surface Temperature and MHW Detection**

84 To detect MHWs for the Arabian Sea, we have used daily NOAA OISST version 2 (Reynolds et al., 2007). The SST data are  
85 analysed for the period of 1982-2019 available on a  $0.25^\circ \times 0.25^\circ$  grid. The MHW detection tool "*heatwaveR*" package  
86 (Schlegel and Smit, 2018) is used for MHW detection. This tool uses the MHW definition based on Hobday et al. (2016) and  
87 characterises MHW as an anomalous, warm, discrete event prolonged for more than five continuous days with SST more than  
88 a particular threshold. The threshold is defined from a fixed seasonal climatological baseline with warmer SST above the 90<sup>th</sup>  
89 percentile of the daily variability. Two consecutive events within three days are considered as a single event. The climatological  
90 baseline is defined based on a fixed 30 year period 1982-2011. This seasonally varying threshold allows heatwaves events to  
91 occur at any season across the year. In order to understand the MHW characteristics, three heatwave metrics are evaluated  
92 here: MHW duration defined as the days between the start and end dates of an event, MHW intensity refers to maximum SST  
93 anomaly during an event, and MHW frequency calculated based on the number of events occur during a season or year.

94

## 95 2.2 Ocean Model

96 The model used in the present study is an ocean general circulation model based on Modular Ocean Model version 5 (MOM5;  
97 Griffies, 2012). The model configuration uses a hydrostatic and Boussinesq approximation. Model coordinates are discretised  
98 based on generalised orthogonal coordinates in horizontal and  $z^*$ -coordinate in the vertical. The model domain extends from  
99 30°E-120°E and 30°S-30°N with a uniform horizontal resolution of 0.25°×0.25° and 40  $z^*$  levels in the vertical. The model  
100 bathymetry is based on Sindhu et al. (2007), with a minimum depth set to 15 m. The horizontal mixing is based on Griffies &  
101 Hallberg (2000), and the vertical mixing scheme is based on Large et al. (1994). The horizontal friction is set to the lowest  
102 value to keep the model stable. The temperature and salinity fields are relaxed to climatological values (Chatterjee et al., 2012)  
103 with a time scale of 30 days within the 4° sponge layer at the open eastern and southern boundaries. Salinity at the surface is  
104 restored with a relaxation of 15 days. To realistically simulate the cross basin flow, the narrow Palk strait between India and  
105 Sri Lanka is closed in this model (Chatterjee et al., 2013, 2017).

### 106 2.2.1 Model experiments and forcing

107 The model is initially spin-up for 35 years from a state of rest, and then the interannual run was carried out for 1990-2018  
108 using restart state of the ocean from the final year simulation of the climatological run. For forcing the model, daily surface  
109 momentum fluxes (zonal and meridional wind stress) and surface heat fluxes (shortwave radiation, longwave radiation, air  
110 temperature and 2 m specific humidity) are obtained from Tropflux data (Praveen et al., 2012, 2013). The precipitation and  
111 surface air pressure are obtained from the NCEP reanalysis product (Kalnay et al., 1996). The monthly climatological river  
112 discharge is based on Vörösmarty et al. (1996) and Papa et al. (2010) and is introduced over the top 15 m of the water column.  
113 The model is extensively validated for the north Indian Ocean in earlier studies (Chatterjee et al., 2013, 2019; Shankar et al.,  
114 2016, 2018; Vijith et al., 2016; Lakshmi et al., 2020). In order to analyse the model simulated anomaly for each variable, this  
115 29-year interannual simulation is used to calculate a climatological field.

### 116 2.2.2 Mixed layer heat budget

117 In order to understand the dominant physical forcing in the genesis of MHWs, a volume-averaged mixed layer heat budget  
118 analysis has been carried out using the temperature and velocity fields taken from the model simulation. The mixed layer  
119 temperature tendency over the time-varying mixed layer and fixed region of area  $A$  is given by

$$\frac{\partial \bar{T}}{\partial t} = \underbrace{-\overline{\nabla_H T}}_{Adv_H} + \underbrace{\frac{1}{\rho C_P} \int_A \frac{Q}{h} dA}_{\bar{Q}_v} - \underbrace{w \frac{\partial \bar{T}}{\partial z} - \frac{1}{Ah} \int_A (k_v \frac{\partial T}{\partial z})}_{Subsurface Process} \quad (1)$$

120 Where  $T$  is the SST,  $t$  is time, and overbar represents volume averaged over the region  $A$  and within the time-varying mixed  
121 layer depth  $h$ .  $Adv_H$  is the horizontal advection of temperature,  $Q$  is the net surface heat flux corrected for shortwave penetration  
122 below the surface mixed layer,  $\rho C_P$  is the specific heat capacity of seawater,  $w$  represents the vertical velocity and  $k_v$  is the

123 vertical eddy diffusivity. The vertical advection and diffusion together represent subsurface processes that influence mixed  
124 layer temperature.

### 125 **3 Trends in the MHW**

126 Figure 1 shows the trend of various MHWs characteristics of the Arabian Sea (north of 5°N). Annually, the number of MHW  
127 days increased significantly over the entire Arabian Sea (Figure 1a). The northern Arabian Sea and the southern Arabian Sea  
128 show the strongest annual increasing trend with a rate of ~3 days/year. A similar increasing trend is also noticeable in the  
129 Persian Gulf and the Gulf of Aden, two marginal seas connected to the Arabian Sea. The rest of the Arabian Sea, including the  
130 coastal water of India, shows an annual increase in the MHW days at a rate of 1.5-2 days/year. We find that pre-monsoon or  
131 spring intermonsoon (PRM; March-April-May) and the summer monsoon (SWM; June-July-August-September) seasons  
132 constitute most of the marine heatwave days observed annually across the years, with about 60% of heatwaves days occurring  
133 during these two seasons in the Arabian Sea. This is the time when the north Indian ocean sees rapid warming (SST can reaches  
134 close to 31°C) as the Inter-Tropical Convergence Zone moves to the northern hemisphere over the Indian landmasses (Joseph,  
135 1990; Vinayachandran and Shetye, 1991; Shenoi et al., 1999; Chatterjee et al., 2012). Notably, the trends of the heatwave days  
136 show marked spatial contrast between the two seasons (Figure 1d, g). During PRM season, the strongest trend is primarily  
137 limited to the northern Arabian Sea along the coast of Pakistan, the northwestern coast of India (coast of Gujarat and  
138 Maharashtra), and the western boundary of the Arabian Sea along the coast of Arabia and Somalia. In comparison, the rest of  
139 the Arabian Sea does not show any notable increase in heatwave days. On the other hand, during SWM, a significant increase  
140 in heatwave days is observed in the southeastern Arabian Sea, particularly all along the west coast of India. Additionally, the  
141 northern Arabian Sea continues to show a significant increasing trend similar to the PRM season but limited mainly along the  
142 coast of Iran, Pakistan and the northeast coast of India. The western Arabian Sea does not show any significant trend in  
143 heatwave days during this season.

144  
145 The spatial heterogeneity in the observed MHWs across the two seasons is owing the underlying differences in the oceanic  
146 dynamics and the air-sea interactions. During PRM, the rapid rise in SST is primarily driven by weaker winds, shallow mixed  
147 layer (~20-30 m; Montégut et al., 2004), the remotely forced propagating Rossby waves (Schott and McCreary, 2001;  
148 Vinayachandran and Shetye, 1991; Rao and Sivakumar, 1999; Shenoi et al., 1999; Durand et al., 2004; Shankar et al., 2004;  
149 Vinayachandran et al., 2007) and the intrusion of the Bay of Bengal freshwater by the coastal currents (Shenoi et al., 1999).  
150 However, by late May, as the summer monsoon winds start to blow over the Arabian Sea, the SST cools rapidly along the  
151 western boundary of the Arabian Sea (Vinayachandran et al., 2021). However, the central and eastern Arabian Sea remains  
152 warm (> 28°C) until July (Chatterjee et al., 2012). By August, SST drops below 28°C over most parts of the Arabian Sea driven  
153 by cloud cover and strong wind-driven mixing (Phillips et al., 2021). It is likely that this mean SST rise during these two  
154 seasons possibly has a significant impact on the MHW genesis over this region and thus, studied separately.

155

156 The frequency of heatwaves also show a marginal annual increasing trend across the Arabian Sea, but the stronger trend of  
157  $\sim 0.06\text{--}0.08$  event/year is limited to the southern and northeastern Arabian Sea and all along the west coast of India (Figure 1b).  
158 During PRM and SWM season, the increasing trend of heatwave frequency is mostly collocated with the regions where an  
159 increasing trend of heatwave days is observed (Figure 1e, h). Therefore, while during the PRM season, an increasing trend in  
160 frequency is observed in the northern Arabian Sea region at a rate of  $\sim 0.1\text{--}0.15$  event/year, the SWM season shows a similar  
161 trend along the west coast of India and across the southeastern Arabian Sea region. Note here that, annually, while the increase  
162 in the number of heatwaves over the four decades is only about 3-4 events, the heatwave days have increased by about 80-120  
163 days. This indicates that the heatwaves have become much prolonged in the recent decade than that of the early 80s' and 90s'.  
164 On the other hand, heatwave intensity shows a meagre increase over most parts of the Arabian Sea. The most intense MHW  
165 intensity is experienced in the northern Arabian Sea, where an increasing rate of  $\sim 0.05^\circ\text{C}/\text{year}$  is observed during the PRM  
166 season.

167

168 Next, in order to understand the heatwave characteristics in detail, based on the observed trend of the various heatwave  
169 characteristics, we have selected two regions in the Arabian Sea for further analysis: the northern Arabian Sea (NAS;  $60^\circ\text{E}\text{--}$   
170  $70^\circ\text{E}, 18^\circ\text{N}\text{--}25^\circ\text{N}$ ) and the southeastern Arabian Sea (SEAS;  $65^\circ\text{E}\text{--}74^\circ\text{E}, 7^\circ\text{N}\text{--}16^\circ\text{N}$ ) (black boxes in Figure 1). Figure 2 shows  
171 the time series of percentage of heatwave days across each year annually and seasons-wise since 1982 for these two selected  
172 regions. In both regions, the number of heatwave days was comparatively low until the year 2000 except for the year 1986/87,  
173 1992 and 1997/1998, coinciding with the initiation phase of the El-Niño and the positive phase of the Indian Ocean Basin  
174 Mode (IOBM). The warmer than usual SST during El-Niño and positive phase of IOBM thus potentially explains these  
175 exceptions. Annually during this pre-2000 era, only  $\sim 5\text{--}10\%$  of days experience heatwaves in these regions. After 2000, the  
176 number of heatwave days increased significantly, with an average of  $\sim 10\text{--}20\%$  days experienced heatwaves in almost all years.  
177 Further, the rapid increase in heatwave days is observed from the year 2015 with at least 25-50% of days experienced  
178 heatwaves. During PRM season, the percentage of heatwave days is marginally higher in the NAS compared to the SEAS  
179 (Figure 2b, e). Moreover, as noted for annual, during PRM season, NAS shows a marked rise in heatwave days from the year  
180 2015 with consistently more than 25-50% of days experienced heatwaves in this region. Nevertheless, during the entire satellite  
181 era, the year 2010 and 2016 stands out as both regions experienced heatwave for almost all days during this season. During  
182 SWM season, the characteristics of heatwave days remain similar as was observed in PRM (Figure 2c, f). The only exception  
183 is that since 2015, SEAS has experienced more heatwave days than the NAS. Notably, the summer of 2015, 2017 and 2019  
184 exhibit at least 50% or more heatwave days in the SEAS.

185

186 Overall, there is a notable increasing trend of the heatwave days annually and for the PRM and SWM seasons. Notably, the  
187 number of heatwaves events annually also increased progressively over the years (Figure 3). The rapid increase in MHW days  
188 and frequency in the last decade coincides with the rapid mean SST warming of this region. This indicates that the

189 anthropogenic warming of the mean SST is likely behind this increased heatwaves over this region. Further, most of the intense  
190 heatwave years also coincide with the El-Niño years, suggesting an important role of climate modes in modulating these  
191 extreme events in this region, which agrees with what is observed in other regional seas across the world ocean (Oliver et al.,  
192 2019).

#### 193 **4 Role of Indian Ocean Warming and SST Variability**

194 The Indian Ocean has been warming rapidly over the last few decades. An estimate based on Enhanced Reconstructed Sea  
195 Surface Temperature (ERSSTv4) indicates that the tropical Indian Ocean is warming at a rate of 0.15°C/decade during 1951-  
196 2015 (Roxy et al., 2020), this is particularly conspicuous during summer months (Roxy et al., 2014). SST trend calculated  
197 during the study period (1982-2019) for the Arabian Sea indicates that annual anomalous warming of ~1.5°C in the recent  
198 decade is limited in the northern part of the Arabian Sea and ~0.75°C in some parts of the southern Arabian Sea (Figure 4a).  
199 However, the season-wise SST trend shows pronounced spatial contrast between PRM and SWM seasons: while during PRM,  
200 NAS experiences anomalous warming of more than ~1.5°C (Figure 4b), during SWM the warming of ~0.75-1°C is located  
201 close to the west coast of India (Figure 4c). Notably, the regions with the strongest warming trend also experience an increasing  
202 trend of MHWs (see Figure 1), indicating that the warming of the mean SST contributes to the increasing trend of heatwave  
203 days in the Arabian Sea. This is in agreement with Oliver et al. (2019), who suggest that about 2/3rd of the global ocean  
204 experiences an increasing trend of heatwave days during the satellite period due to the rising mean temperature of the ocean.  
205 The use of a fixed climatological baseline in this (and other) studies inherently means that rapid warming in the recent decade  
206 shifted the mean SST towards the heatwave threshold.

207  
208 In order to understand the importance of the mean SST trend and the variability in the SST on the heatwave days over the  
209 Arabian Sea, the SST time series is decomposed as below:

$$T(t) = T^{tr}(t) + T^{var}(t), \quad (2)$$

210 here,  $T(t)$  is the time series of SST,  $T^{tr}(t)$  is the SST trend, and  $T^{var}(t)$  is the SST anomaly after removing the trend. Figure  
211 5 shows the time series of the percentage of heatwave days based on detrended SST time series ( $T^{var}$ ). In this case, the duration  
212 of MHWs for each year and season is primarily driven by SST variability. The major contrast between heatwave days based  
213 on  $T(t)$  and  $T^{var}(t)$  (compare Figures 2 and 5) is that there is no secular trend in the heatwave days when calculated based  
214 on only SST variability. This supports that the increasing trend in the MHW days in the Arabian Sea is driven by the rising  
215 temperature of the mean SST and not the variability. It should be noted that the detection of MHWs is relative to a fixed  
216 baseline. If one were to use a moving baseline, warming SSTs would not necessarily lead to a trend in MHW days. Note also  
217 that SST variability contributed most strongly during the PRM season of 2010 in the NAS region, with almost 50-75% of days  
218 of this season experiencing heatwaves due to SST variability (Figure 5b). The 2016 event was the second strongest event in  
219 this region, contributed strongly by the SST variability. In fact, as the next section shows, we find that El-Niño primarily drives

220 these large number of heatwave days during PRM season via the positive phase of the Indian Ocean Basin mode. In contrast,  
 221 in the SEAS, the SST variability contributed most for the year 2016 with almost 20-40% of the observed heatwave days. The  
 222 other notable years are 1988, 1998 and 2003, when a considerable number of days experience heatwave in this region due to  
 223 SST variability alone. On the other hand, during the SWM season, the contribution of SST variability is most notable for the  
 224 years 1982, 1983, 1987, 1988, and 2010 in the NAS and the years 1983, 1987, 2003 and 2015 in the SEAS.

225

226 In order to compare the role of mean SST warming with the SST variability, Figure 6 shows that the time series of the ratio of  
 227 the heatwave days owing to the SST trend and its variability by approximating Equation (2) as follows:

$$\frac{MHW(T^{tr})}{MHW(T^{var})} \approx \frac{MHW(T)}{MHW(T^{var})} - 1, \quad (3)$$

228 assuming that MHW based on  $T^{tr}$  and  $T^{var}$  are independent of each other. This is a fairly good approximation as the seasonal  
 229 climatology is prepared using a 30-year record and doesn't include the last decade when a rapid increase in SST is observed.  
 230 Thus, it can provide useful insights of the role of the mean warming trend of SST on the MHW generation. It shows a very  
 231 secular shift after the year 2000 in the driving force of the total annual heatwave days in the Arabian Sea. While, during the  
 232 pre-2000 era, the natural variability of SST contributes most in driving the MHWs, post-2000, the warming trend of mean SST  
 233 becomes the dominant factor. It also shows that the influence of mean SST warming increased very rapidly over the last two  
 234 decades, which is expected to continue further under the unabated Indian Ocean warming. However, there are years when the  
 235 ratio is much smaller when the climate mode driven variability contributes significantly to these extreme warm events as noted  
 236 in Figure 5.

## 237 **5 Role of Dominant Climate Modes**

238 Indian Ocean dipole mode (IOD) and El-Niño Southern Oscillation (ENSO) are the two dominant climate modes that  
 239 contribute to the SST variability of the tropical Indian Ocean in interannual timescale (Saji et al., 1999; Du et al., 2009). During  
 240 the positive phase of the IOD, the western Indian Ocean shows anomalous warming, whereas the eastern Indian Ocean cools.  
 241 In the negative phase, the sign of the SST anomaly reverses. Similarly, ENSO modulates the SST in the tropical Pacific, but  
 242 the influence of ENSO can be felt in other basins as well through an atmospheric teleconnection via anomalous Walker  
 243 circulation (Du et al., 2009; Roxy et al., 2014) and the inter-basin transport of water mass properties (Lee et al., 2015). During  
 244 the positive phase of ENSO, i.e. during El-Niño, the western Indian Ocean shows warmer anomaly due to the weakening of  
 245 the summer monsoon winds and increased shortwave radiation (Swapna et al., 2014). On the other hand, during La-Nina, most  
 246 parts of the Indian Ocean experience cooler anomaly except the west coast of Australia where SST elevated due to heat  
 247 transport via Leeuwin current (Feng et al., 2013; Benthuyzen et al., 2014). Note here that many IOD co-occurred with ENSO,  
 248 and therefore, atmospheric teleconnections associated with ENSO are often considered to be one of the primary triggers of the  
 249 IOD events (Allan et al., 2001). Nevertheless, there are many instances when extreme IOD appears in the absence of ENSO,



250 suggesting the importance of regional processes within the Indian Ocean in the evolution of IOD (Ashok et al., 2003). However,  
251 considering the strong coupling between the ENSO and IOD mode, separating the effects of these modes on the Indian Ocean  
252 warming sometimes becomes challenging.

253

254 Additionally, associated with the direct impact of ENSO, the Indian Ocean warming mode (also referred to as Indian Ocean  
255 Basin mode; IOBM), which peaks during the decaying phase of the El-Niño and after the La-Nina, also contributes to the  
256 widespread warming of the tropical Indian Ocean (Xie et al., 2009). Notably, the initiation of IOBM mode is primarily caused  
257 by the ENSO induced suppressed atmospheric convection over the tropical Indian Ocean (Klein et al., 1999). However, it can  
258 act as a capacitor to influence atmospheric teleconnection till next summer in the decaying phase of the El-Niño (Xie et al.,  
259 2009). Hence, the warming of the Indian Ocean during the positive IOBM mode inherently contains the effect of previous El-  
260 Niño.

261

262 Similarly, North Atlantic Oscillation (NAO) has also been shown to play an important role in modulating SST of the Indian  
263 ocean in interannual to decadal time scale (Xie et al., 2021). Therefore, these climate modes can support the genesis or  
264 suppression of heatwaves depending upon their phases via modulating the thermocline depth and associated air-sea interactions  
265 of the basin (Holbrook et al., 2019, 2020; Oliver et al., 2021).

266

267 This section will look at the role of these climate modes, particularly IOD, ENSO, IOBM and NAO, on the genesis of MHWs  
268 in the Arabian Sea. As noted already in the previous section, the most number of heatwave days observed either during the  
269 initiation phase of El-Niño or during the decaying phase of the El-Niño (i.e. during the positive phase of the IOBM).

270 This indicates that the El-Niño and IOBM climate modes play a significant role in modulating heatwaves in this region. Figure  
271 7a shows the correlation between MHW days derived from the detrended SST observation and the climate modes. ENSO  
272 shows the strongest correlation in the southcentral Arabian Sea with a correlation coefficient of  $\sim 0.5$ . The correlation decreases  
273 northward and, in fact, turns negative in the Persian Gulf region. This is in line with the correlation between Indian Ocean  
274 SST warming and the El-Niño mode (Roxy et al., 2014). The influence of IOD is most prominent in the western Arabian Sea  
275 in the vicinity of the western box of the IOD. Otherwise, the correlation is generally weak for the rest of the basin except close  
276 to the coast of Iran and Pakistan where a marginal increase in correlation is observed. However, note here that, unlike ENSO,  
277 the spatial and temporal length scale of IOD is much smaller. Thus, the correlation across the entire year may be less, but it  
278 can still significantly influence a larger region during its peak phase. As expected, the IOBM, which represents the basin-wide  
279 warming mode of the tropical Indian Ocean, shows the strongest influence on the MHW days with a correlation coefficient of  
280  $\sim 0.5$  in most parts of the Arabian Sea. In this case also, like ENSO, the correlation decreases in the north. The influence of  
281 NAO is the weakest among the other climate modes and is mostly limited to the SEAS region close to the southern part of the  
282 west coast of India during its negative phase.

283

284 As evident in the correlation map, the strong association of IOBM with the MHW days is also reflected in the large percentage  
285 of heatwaves days that co-occur with the positive phase of the IOBM (Figure 7b). Annually, about 60% and 75% of heatwave  
286 days co-occur with the positive IOBM in the NAS and SEAS, respectively. These co-existing numbers go much higher during  
287 the PRM season with more than 82% of heatwave days coincide with the positive IOBM phase in the SEAS region. The next  
288 most influencing climate mode is the positive phase of ENSO or El-Niño. This is more conspicuous during the PRM season  
289 as both the region experiences close to 50% co-existence between heatwave days and El-Niño. On the other hand, positive  
290 IOD also significantly co-exist with more than 40% of heatwave days during this season. During the SWM season, this  
291 association between IOBM and heatwaves decrease a bit with about 43% and 68% of heatwave days co-occur with the positive  
292 IOBM in the NAS and SEAS, respectively. The influence of El-Niño, on the other hand, show a marked difference between  
293 NAS and SEAS region. During summer, while in the SEAS, El-Niño co-occurs with ~50% heatwave days; in the NAS, both  
294 the phase (i.e. El-Niño and La-Nina) co-occur in ~20% heatwave days. This equal co-occurrence of heatwave days in NAS  
295 indicates that there is no causal relationship between heatwave and ENSO in this region and therefore, possibly a mere  
296 coincidence. A similar relationship is observed for the IOD mode as well i.e. heatwaves during its positive and negative phase  
297 co-occur for an almost similar number of days and thus, hinted that IOD most likely doesn't cause heatwaves in the NAS  
298 during summer months. On the other hand, as seen in the correlation maps, the negative phase of NAO likely contributes to  
299 the genesis of MHWs in the SEAS with close to 20% of heatwave days coinciding with this mode during this season.

## 300 **6 Dynamical mechanisms inferred from a case study**

301 The dynamical processes responsible for the genesis of MHWs across the global ocean vary significantly (Holbrook et al.,  
302 2019). Moreover, the processes may differ from one event to the other in a particular region. For example, different processes  
303 were involved in the consecutive observed MHW events in the South China Sea during 2016-2018 (Gao et al., 2020), in the  
304 northeast Pacific during 2014-15 (Di Lorenzo et al., 2016) and 2019-20 (Chen et al., 2021) or along the southeastern Australian  
305 coast (Oliver et al., 2016; Li et al., 2020). The Arabian Sea also exhibits similar heterogeneity in the processes responsible for  
306 the genesis of MHWs across the seasons/years (more details are given in the discussion section). In this study, we analysed  
307 the heatwave event during the year 2010 as it was the longest observed event since the availability of the satellite observations  
308 and lasted for about 60-70 days (Figure 8 and 9). The initiation of the heatwave appears sometime in the last week of March  
309 in the northern and northeastern parts of the Arabian Sea when the SST is hovering around 27-29°C, i.e. about 0.5°C more than  
310 the threshold (Figure 10). By the third week of April, the heatwave event covers the entire northern part of the Arabian Sea.  
311 By May, with the northward movement of ITCZ, the entire Arabian Sea turns very warm with SST more than 31°C. This  
312 intensifies the heatwave further to its peak and spreads along the western part of the Arabian Sea along the coast of Arabia  
313 with an intensity of ~2°C. By the end of May, a low-level southwesterly surface wind (also known as Findlater Jet; Findlater,  
314 1969) start to blow along the coast of Somalia, causing water to upwell along the coast (Schott and McCreary, 2001; Chatterjee  
315 et al., 2019; Vinayachandran et al., 2021). As the summer monsoon winds intensify, the upwelling signature extends all along

316 the western boundary of the Arabian Sea. Thus, leading to a rapid decrease in SST in the western Arabian Sea, cause the  
317 heatwave to limit in the northeastern Arabian Sea close to the northwest coast of India. Finally, by mid-June, the heatwave  
318 event wanes off as the summer monsoon clouds set in across the western ghats of India. The onset of summer monsoon clouds  
319 reduce the shortwave radiation, thus contribute to the decreasing temperature and termination of the heatwave.

320

321 The dominating processes involved in the generation of surface heatwaves in a particular region can be assessed through the  
322 analysis of heat sources and sinks in the upper mixed layer, which ultimately reflects in the variation of the SST. This approach  
323 was employed earlier for the understanding of the evolution of heatwaves during the 2011 Ningaloo Nino off Western Australia  
324 (Benthuisen et al., 2014), during 2012 warming off northeastern America (Chen et al., 2014) and in the East China Sea and  
325 the south Yellow Sea during the summer of 2016-2018 (Gao et al., 2020). Here, we have used a similar mixed layer heat  
326 budget formulation for the Arabian Sea (see Equation 1) to understand the dominant physical processes that likely favour this  
327 heatwave event's generation. The model could simulate the rapid rise of SST during this period, albeit with a cold bias of about  
328 0.5°C (Figure 10). The spatial pattern of SST is also captured by the model quite well throughout the season (Figure 8 and 9),  
329 proving reasonable confidence to the mixed layer budget based on this model simulation. Note, however, that model is failed  
330 to simulate very short timescale SST variation (day-to-day), likely due to its resolution and coarser atmospheric flux used to  
331 force the model simulations.

332

333 Figure 11 shows the mixed layer heat budget at a point (63°E/19°N) located in the northcentral Arabian Sea and central to the  
334 NAS box. SST tendency starts to peak up by mid-March as the mixed layer soals to about 20 m over most of the Arabian Sea  
335 (Figure 12a), driven by weaker winds (Figure 13). The weaker winds further add to the weakening of the evaporative cooling  
336 resulting in an increase in the net surface heat flux ( $Q_v$ ) (Figure 11) and therefore, rapid increase in SST (Figure 10). However,  
337 strong intraseasonal variability is evident primarily driven by the net surface heat flux ( $Q_v$ ) owing to the intraseasonal  
338 variability in the surface winds. The anomalously shallow mixed layer during the pre-monsoon of 2010 (Figure 12b), owing  
339 to the weaker than normal winds driven by El-Niño atmospheric teleconnection, exaggerate the warming compared to the other  
340 years. The warming rate peaks in late April to early May as the  $Q_v$  continues to increase over the entire basin (Figure 11). As  
341 the summer monsoon winds peak up (Figure 13), thermocline deepens, and SST cools due to enhanced entrainment of cold  
342 subsurface water to the upper water column (Figure 11). Additionally, enhanced wind speed increases the latent heat loss  
343 (Figure 13) that further adds to the sharp decrease in  $Q_v$  and therefore, contributes to the further cooling of SST (Figure 10).  
344 In the subsequent days, SST recovers a bit with a weakly positive tendency before a sharp drop again on 1st June, 2010 driven  
345 by negative  $Q_v$  and strong entrainment cooling (Figure 11). This sharp drop in SST is linked to a severe cyclone *Phet*. The  
346 tropical cyclonic storm *Phet* first developed on 31st May, 2010 in the central Arabian Sea around 1000 km west of Mumbai.  
347 It attends its peak wind speed of about 230 km/hr on 2nd June, 2010 and made landfall in eastern Oman on 3rd June, 2010  
348 (See panel for 2nd June of Figure 8 for the cyclone track). The SST along this cyclone track decrease rapidly (more than 1°C)  
349 and is contributed significantly to the weakening of the persisting heatwave in this region (Figure 9). After this cyclone, the

350 SST recovers slightly but remains relatively cooler (Figure 10) due to the gradual decrease in shortwave flux and enhanced  
351 latent heat loss (Figure 13). It indicates that the cyclone *Phet* played a significant role in terminating the persisting heatwave  
352 in a large part of the western Arabian Sea. Finally, the following intensification of summer monsoon winds and reduction in  
353 shortwave flux due to cloud cover reduces the SST further, resulting in the waning of the heatwave event from the northern  
354 Arabian Sea.

## 355 **7 Summary and discussion**

356 In this study, we have investigated the trends and genesis of the MHWs in the Arabian Sea (north of 5°N). Particularly we  
357 studied the three primary metrics of heatwaves: duration, frequency and intensity for the period of 1982-2019 and rallied  
358 primarily on the OISSTv2 SST observations. Further, we have carried out a case study for the longest heatwave events during  
359 the study period using an ocean model simulation based on Modular Ocean Model version 5 (MOM5) for understanding the  
360 underlying forcing mechanism in the genesis of such heatwave events.

361  
362 Like other regions of the world ocean, we find that the Arabian Sea also experiences a rapid increase in heatwave days. At the  
363 same time, heatwave frequency shows a marginal increase, suggesting that the heatwaves have now become prolonged and,  
364 in fact, sometimes persistent for an entire season in the recent decade. However, due to the weaker SST variability in this basin,  
365 a consequence of equatorial proximity, there is no significant increase in the heatwave intensity, a parameter often used to  
366 mark these events. Thus, this region remained unexplored in terms of MHWs in other global studies. The increasing trend of  
367 heatwave days is mainly evident post-2000 era and became conspicuous after 2015.

368  
369 A detailed study for the pre-monsoon (or spring intermonsoon) and the summer monsoon indicates that the heatwave trend  
370 varies significantly across the seasons. During pre-monsoon, an increase in heatwave days at a rate of 15-20 days/decade is  
371 evident are primarily in the northern part of the Arabian Sea and along the coast of Arabia. However, during summer, the  
372 increasing trend at a similar rate is evident all along the coast of India and over a large part of the southeastern Arabian Sea.  
373 Noticeably, across the last four decades, the years 2010 and 2016 show the longest heatwave days as the strong El Nino, on  
374 top of the mean warming trend, caused large and persistent warm SST across the Arabian Sea. An analysis of heatwave days  
375 based on detrended SST anomaly suggests that the enormous trend in the observed heatwave days are primarily linked to the  
376 rise in the mean SST of the Arabian Sea. The switch between the dominance of SST variability and the mean SST warming  
377 happened sometime around 2000. However, SST variability still contributes significantly for the years when climate variability  
378 is dominated by major climate modes and cause a significant source of SST warming in this basin. A detailed study of the  
379 association of heatwave days and these climate modes indicates that the Indian Ocean Basin mode (also referred to as Indian  
380 Ocean warming mode) via the decaying phase of the El-Niño influence very strongly influences the genesis of MHWs. In fact,  
381 during pre-monsoon, when this Indian Ocean Basin Mode is most active, it co-exists in more than 70-80% of heatwave days.

382 During the summer monsoon, its influence weakens over the entire Arabian Sea but remains significantly prominent in the  
383 southeastern Arabian Sea. However, co-existing days are reduced to merely 40% in the northern part, as evident in the  
384 correlation maps. The next most influencing climate modes are found to be El-Niño and positive IOD. These modes contribute  
385 to about 40-50% of heatwave days in the northern Arabian Sea during pre-monsoon. During the summer monsoon, the impact  
386 of these climate modes are relatively weaker but still contribute to more than 40% of heatwave days in the southeastern Arabian  
387 Sea. But, in the north, the influence of El-niño and IOD is almost negligible during this season. It is noteworthy here that the  
388 longest heatwave event in the Arabian Sea is noted during spring 2010, which is also coincided with the strongest central  
389 Pacific El-Niño in the recent decades (Lee and McPhaden, 2010). In fact, the central Pacific El-niños seem to have a greater  
390 impact over the Indian Ocean and, therefore, on the Indian monsoon rainfall (Krishna Kumar et al., 2006). The severe drought  
391 during the summer of 2009 is one such example. More generally, with ENSO and IOBM forcing of the Indian Ocean regions,  
392 other environmental hazards (for example, droughts over the Indian subcontinent) will co-occur with MWHs. Therefore,  
393 adaptation strategies will potentially need to account for the societal impacts of multiple co-occurring environmental stressors  
394 on land and in the ocean related to climate variability and change.

395  
396 The heatwave genesis and its forcing mechanisms vary considerably from year to year and within the Arabian Sea. A mixed  
397 layer heat budget shows a substantial heterogeneity in the forcing mechanisms of the genesis of MHWs in the Arabian Sea  
398 (Figure not shown). Considering that case studies designed for a particular heatwave event are necessary for such  
399 understanding, we analyse the possible forcing mechanisms for the longest (~70 days) and one of the intense (~2°C) heatwaves  
400 over the study period observed during the pre-monsoon of the year 2010. Owing to the positive wind-evaporation-SST  
401 feedback during El-Niño of 2009-10 (Du et al., 2009), the 2010 springtime SST in the Arabian Sea show a strong positive  
402 tendency, leading to the formation of one of the strongest heatwaves in the recent decade (Figure 8). The heatwave starts to  
403 decay in the western Arabian Sea with the initiation of summer monsoon winds in the northern Indian Ocean. The upwelled  
404 water along the coast of Arabia limits the heatwave in the northeastern part of the Arabian Sea by late May. The decrease in  
405 net surface heat flux due to enhanced latent heat loss and reduced shortwave flux adds to the rapid cooling of SST during this  
406 period. Finally, the wind steering driven cooling, associated with tropical cyclone *Phet* and subsequent intensification of  
407 summer monsoon, weakens the heatwave further.

408  
409 A similar process is also observed in the late spring of 2020 when a severe cyclone *Nisagra*, which made landfall in Mumbai  
410 (a city located on the west coast of India), caused severe destruction by means of loss of life and property over a vast area,  
411 ended a one half month persistent heatwave of intensity more than 1°C along the west coast of India (Figure 14 and 15).  
412 Interestingly, when we wrote this paper, another severe cyclone *Tauktae* hit the west coast of India and caused extensive  
413 damage to the property and life. This time, the SST was again more than 31°C off the west coast of India. These similar events  
414 suggest that persistent extreme warm conditions like heatwaves may be linked to the increased cyclogenesis over the Arabian  
415 Sea in the recent decade. In fact, as the number of heatwave days increased significantly over the last two decades, the number

416 of tropical cyclones also increased over the Arabian Sea (Figure 14), indicating a clear association between the heatwaves and  
417 the increased cyclogenesis in the Arabian Sea. In a recent study using a longer record, Deshpande et al. (2021) reported a 52%  
418 increase in the frequency of cyclonic storms over the Arabian Sea in recent decades. Further study is required to understand  
419 the dynamical links between heatwaves and associated atmospheric conditions to the observed enhanced cyclogenesis of this  
420 region.

421  
422 This rapid increase in heatwave days in the northern and southeastern Arabian Sea is also likely to cause a severe impact on  
423 the physio-biogeochemical processes of this basin. One such possible impact is the recent increase in the harmful algal bloom  
424 in the Arabian Sea. Recent studies suggest that there is a manyfold increase in the harmful phytoplankton blooms in the  
425 northern Arabian Sea and along the west coast of India attributed primarily to the increased stratification, weaker winds and  
426 warming of the Arabian Sea (Padmakumar et al., 2012; Al Shehhi et al., 2014; Goes et al., 2020). Considering that the region  
427 of increased toxic blooms are collocated with the regions where the heatwave days are observed, the possibility that the relation  
428 between these heatwave events and the triggering of harmful blooms can not be neglected.

429  
430 It is noteworthy that the heatwaves extremes are defined here using a fixed baseline of 1982-2011. Hence, considering that the  
431 recent decades have experienced a rapid rise in SST, the overall SST running mean is shifted more towards the heatwave  
432 threshold in the recent past. Therefore, if one were to use a moving baseline, warming SSTs would not necessarily lead to a  
433 trend in MHW days. The construct of MHW definition should take into account the ultimate impact we intend to address. The  
434 fixed baseline is possibly better suited when the impact on marine biology or atmospheric phenomena like cyclones are  
435 considered. Whereas the moving baseline may be a better choice if the effects of the warming trend are to be avoided. The  
436 implication of various such heatwave definitions is discussed in Oliver et al. (2021).

437  
438 In summary, this study documented marine heatwaves and their various characteristics in the Arabian Sea. This is the first  
439 study where a detailed analysis of marine heatwave for the Arabian Sea, particularly for the coastal water of economic  
440 importance, is discussed. This study advocates further investigation of the impact of heatwave events on the coastal ecosystems  
441 and other oceanic properties of this tropical basin.

#### 442 **Author contribution**

443 AC designed the study and wrote the paper, AC and GA performed the data analysis, LRS conducted the model experiments.  
444 All authors contributed to developing the research and contributed to the discussion.

445 **Competing interests**

446 The authors declare no competing interests.

447 **Data availability**

448 The daily OISST is obtained from <https://coastwatch.pfeg.noaa.gov/erddap/>. The daily north Atlantic oscillation index was  
449 provided by by NCEP Climate Prediction Centre (<https://ftp.cpc.ncep.noaa.gov/cwlinks/>). The best track data for cyclones are  
450 obtained from the "Best Track Archive" of the Joint Typhoon Warning Centre. The model simulations will be made available  
451 upon request. The marine heatwave detection tool heatwaveR was taken from  
452 <https://robwschlegel.github.io/heatwaveR/index.html>.

453 **Acknowledgement**

454 The lead author thank the support provided by the Indian National Centre for Information Services (INCOIS), Ministry of  
455 Earth Sciences, to carry out this research. Funding for this work was provided from the "Deep Ocean Mission" programme of  
456 the Ministry of Earth Sciences, Government of India. The model simulations are carried out in the Ministry of Earth Science's  
457 central HPC facility, "MIHIR". A part of this work was based on the master's dissertation thesis of GA conducted at INCOIS.  
458 LRS was supported by the funding from INSPIRE DST fellowship. We acknowledge the critical comments from two  
459 anonymous reviewers; their comments have helped improve the paper significantly. Plotting and data analysis were carried  
460 out using R and Ferret software. This is INCOIS contribution number 0000.

461 **References**

- 462 Ajayamohon, R. S. and Suryachandra A. R.: Indian Ocean Dipole Modulates the Number of Extreme Rainfall Events over  
463 India in a Warming Environment, *J. Met. Soc. Japan*, 1, 245-252, 2008.
- 464 Al Shehhi, M. R., Gherboudj, I., Ghedira, H.: An overview of historical harmful algae blooms outbreaks in the Arabian Seas.  
465 *Mar Pollut Bull.*, 86 (1-2), 314-324, 10.1016/j.marpolbul.2014.06.048, 2014.
- 466 Allan, Robert J. and Chambers, Don and Drosowsky, Wasyl and Hendon, Harry and Latif, Mojib and Nicholls, Neville and  
467 Smith, Ian and Stone, Roger C. and Tourre, Yves: Is there an Indian Ocean dipole and is it independent of the El Niño-  
468 Southern Oscillation? *CLIVAR Exchanges*, 6 (3), 2001. pp. 18-22. ISSN 1026-0471
- 469 Arias- Ortiz, A., Serrano, O., Masqué, P., Lavery, P. S., Mueller, U., Kendrick, G. A., Rozaimi, M., Esteban, A.,  
470 Fourqurean, J. W., Marbà, N., Mateo, M. A., Murray, K., Rule, M. J., and Duarte C. M.: A marine heatwave drives massive  
471 losses from the world's largest seagrass carbon stocks. *Nat. Clim. Change* **8**, 338–344, [https://doi.org/10.1038/s41558-018-](https://doi.org/10.1038/s41558-018-0096-y)  
472 0096-y, 2018.

473 Ashok, K., Guan, Z., and Yamagata, T. (2003), Influence of the Indian Ocean Dipole on the Australian winter rainfall,  
474 *Geophys. Res. Lett.*, 30, 2003. doi:10.1029/2003GL017926

475 Benthuisen, J., Feng, M. & Zhong, L.: Spatial patterns of warming off Western Australia during the 2011 Ningaloo Nino:  
476 Quantifying impacts of remote and local forcing. *Cont. Shelf Res.*, 91, 232-246, 2014.

477 Benthuisen, J. A., Oliver, E. C. J., Feng, M., and Marshall, A. G. Extreme marine warming across tropical Australia during  
478 austral summer 2015–2016, *J. Geophys. Res.* 123, 1301–1326, 2018.

479 Bond, N. A., Cronin, M. F., Freeland, H., and Mantua, N.: Causes and impacts of the 2014 warm anomaly in the NE Pacific.  
480 *Geophys. Res. Lett.*, 42, 3414–3420, 2015.

481 Caputi, N., Kangas, M., Denham, A., Feng, M., Pearce, A., Hetzel, Y., Arani, C.: Management adaptation of invertebrate  
482 fisheries to an extreme marine heatwave event at a global warming hot spot, *Ecology and Evolution*, 6(11), 3583–3593,  
483 <https://doi.org/10.1002/ece3.2137>, 2016.

484 Chatterjee, A., Shankar, D., Shenoi, S., Reddy, G., Michael, G., Ravichandran, M., Gopalkrishna, V. V., Rao, E. P. R., Bhaskar,  
485 T. V. S. U., and Sanjeevan, V. N. : A new atlas of temperature and salinity for the North Indian Ocean, *Journal of Earth  
486 System Science*, 121(3), 559–593, 2012.

487 Chatterjee, A., Shankar, D., McCreary, J., and Vinayachandran, P.: Yanai waves in the western equatorial Indian Ocean,  
488 *Journal of Geophysical Research: Oceans*, 118, 1556–1570, <https://doi.org/10.1002/jgrc.20121>, 2013.

489 Chatterjee, A., Shankar, D., McCreary, J., Vinayachandran, P., and Mukherjee, A.: Dynamics of Andaman Sea circulation and  
490 its role in connecting the equatorial Indian Ocean to the Bay of Bengal. *Journal of Geophysical Research: Oceans*, 122,  
491 3200–3218. <https://doi.org/10.1002/2016JC012300>, 2017.

492 Chatterjee, A., Kumar, B. P., Prakash, S., and Singh, P.: Annihilation of the Somali upwelling system during summer monsoon,  
493 *Scientific reports*, 9(1), 7598. <https://doi.org/10.1038/s41598-019-44099-1>, 2019.

494 Chen, K., Gawarkiewicz, G. G., Lentz, S. J., Bane, J. M.: Diagnosing the warming of the northeastern U.S. coastal ocean in  
495 2012: a linkage between the atmospheric jet stream variability and ocean response, *J. Geophys. Res. Oceans*, 119:218–27,  
496 2014.

497 Chen, Z., Shi, J., Liu, Q., Chen, H., and Li, C.: A persistent and intense marine heatwave in the Northeast Pacific during 2019–  
498 2020. *Geophysical Research Letters*, 48, e2021GL093239, 2021. <https://doi.org/10.1029/2021GL093239>.

499 Chowdary, J. S. and Gnanaseelan, C.: Basin-wide warming of the Indian Ocean during El Niño and Indian Ocean dipole years,  
500 *Int. J. of Clim.*, 27, 1421-1438, <https://doi.org/10.1002/joc.1482>, 2007, 2007.

501 Chakravorty, S., Chowdary, J. S., Gnanaseelan, C.: Epochal changes in the seasonal evolution of Tropical Indian Ocean  
502 warming associated with El Niño, *Climate Dynamics*, 42, 805-822, doi:10.1007/s00382-013-1666-3, 2014.

503 Cavole, L. M., Alyssa, M. D., Rachel, E. D., Ashlyn, G., Irina, K., Camille, M. L. S. P., May-Linn, P., Arturo, R.-  
504 V., Sarah, M. S., Nicole, K. Y., Michelle, E. Z., and Peter, J.S.: Biological Impacts of the 2013–2015 warm- water  
505 anomaly in the northeast Pacific: winners, losers, and the future, *Oceanography*, 29, 273–285,  
506 <https://doi.org/10.5670/oceanog.2016.32>, 2016.



507 CMFRI, 2007a. Marine fisheries profile India, <http://www.cmfri.org.in/data-publications-/5/2007>.

508 Deshpande, M., Singh, V.K., Ganadhi, M.K. et al. Changing status of tropical cyclones over the north Indian Ocean. *Clim Dyn*  
509 57, 3545–3567 (2021). <https://doi.org/10.1007/s00382-021-05880-z>

510 Du, Y., Xie, S.-P., Huang, G. and Hu, K.: Role of air–sea interaction in the long persistence of El Niño–induced North Indian  
511 Ocean warming. *J. Climate*, **22**, 2023–2038, 2009.

512 Durazo, R., and Baumgartner, T. R.: Evolution of oceanographic conditions off Baja California. *Prog. Oceanogr.* 54, 7–31,  
513 2002.

514 Durand F, Shetye SR, Vialard J, Shankar D, Shenoi SSC, Ethe C, Madec G.: Impact of temperature inversions on SST evolution  
515 in the Southeastern Arabian Sea during the pre-summer monsoon season. *Geophys Res Lett* 31:L01305, 2004.  
516 doi:10.1029-2003,GL018906

517 Feng, M., M. J. McPhaden, S.-P. Xie, and J. Hafner, 2013: La Niña forces unprecedented Leeuwin Current warming in 2011.  
518 *Nature Sci. Repts.*, 3, 1277, doi 10.1038/srep01277.

519 Findlater, J.: Mean monthly air flow at low levels over the western Indian ocean. *Geophys. Mem.* 115, 1969.

520 Gao, G., Marin, M., Feng, M., Yin, B., Yang, D., Feng, X., Ding, Y., Song, D.: Drivers of marine heatwaves in the East China  
521 Sea and the South Yellow Sea in three consecutive summers during 2016–2018, *Journal of Geophysical Research:Oceans*,  
522 125, e2020JC016518, <https://doi.org/10.1029/2020JC016518>, 2020.

523 Goes, J.I., Tian, H., Gomes, H.d.R., Anderson, O. R., Khalid, A.-H., deRada, S., Luo, H., Lubna, A.-K., Adnan, A.-A.,  
524 Martinson, D. G.: Ecosystem state change in the Arabian Sea fuelled by the recent loss of snow over the Himalayan-Tibetan  
525 Plateau region. *Sci. Rep.*, 10, 7422, <https://doi.org/10.1038/s41598-020-64360-2>, 2020.

526 Griffies, S.M., and Hallberg, R.W.: Biharmonic friction with a Smagorinsky-like viscosity for use in large-scale eddy-  
527 permitting ocean models, *Monthly Weather Review*, 128(8), 2935–2946, 2000.

528 Griffies, S. M.: Elements of the modular ocean model (MOM), GFDL Ocean Group Tech. Rep, 7, 620, 2012.

529 Hobday, A. J., Alexander, L. V., Perkins, S. E., Smale, D. A., Straub, S. C., Oliver, E. C. J., Benthuisen, J. A., Burrows, M.  
530 T., Donat, M. G., Feng, M., Holbrook, N. J., Moore, P. J., Scannell, H. A., Gupta, A. S., Wernberg, T.: A hierarchical  
531 approach to defining marine heatwaves, *Prog. Oceanogr.*, 141:227–38, 2016.

532 Holbrook, N. J., Scannell, H. A., Gupta, A. S., Benthuisen, J. A., Feng, M., Oliver, E. C. J., Alexander, L. V., Burrows, M.  
533 T., Donat, M. G., Hobday, A. J., Moore, P. J., Perkins-Kirkpatrick, S. E., Smale, D. A.,  
534 Straub, S. C., Wernberg, T.: A global assessment of marine heatwaves and their drivers. *Nat. Commun.* 10:2624, 2019.

535 Holbrook, N.J., Sen Gupta, A., Oliver, E.C.J., Hobday, A. J., Benthuisen, J. A., Scannell, H. A., Smale, D. A., and Wernberg,  
536 T.: Keeping pace with marine heatwaves, *Nat. Rev. Earth Environ.*, 1, 482–493, [https://doi.org/10.1038/s43017-020-0068-](https://doi.org/10.1038/s43017-020-0068-4)  
537 4, 2020.

538 Hughes, T. P., Kerry, J. T. and Wilson, S. K.: Global warming and recurrent mass bleaching of corals. *Nature*, 543, 373–377,  
539 <https://doi.org/10.1038/nature21707>, 2017.

540 Joseph, P. V.: Warm pool over the Indian Ocean and monsoon onset, *Trop. Ocean Atmos. Newsl.*, Winter, 53, 1 – 5, 1990.

541 Kalnay, E., Kanamitsu, M., Kistler, R., Collins, W., Deaven, D., Gandin, L., Iredell, M., Saha, S., White, G., Woollen, J., Zhu,  
542 Y., Chelliah, M., Ebisuzaki, W., Higgins, W., Janowiak, J., Mo, K. C., Ropelewski, C., Wang, J., Leetmaa, A., Reynolds,  
543 R., Jenne, R., and Joseph, D.: The NCEP/NCAR 40-year reanalysis project, *Bull. Am. Meteorol. Soc.*, **77**, 437–471, 1996.

544 Klein, S. A., Soden, B. J. and Lau, N.-C.: Remote sea surface temperature variations during ENSO: Evidence for a tropical  
545 atmospheric bridge. *J. Climate*, **12**, 917–932, 1999.

546 Kumar, K. K., Rajagopalan, B., Hoerling, M., Bates, G., and Cane, M.: Unraveling the mystery of Indian monsoon failure  
547 during El Nino. *Science*, **314**, 115– 119, <https://doi.org/10.1126/science.1131152>, 2006.

548 Lakshmi, R. S., Chatterjee, A., Prakash, S., and Mathew, T.: Biophysical interactions in driving the summer monsoon  
549 chlorophyll bloom off the Somalia coast. *Journal of Geophysical Research: Oceans*, **125**,  
550 <https://doi.org/10.1029/2019JC015549>, 2020.

551 Large, W. G., McWilliams, J. C., and Doney, S. C.: Oceanic vertical mixing: A review and a model with a nonlocal boundary  
552 layer parameterisation. *Reviews of Geophysics*, **32**(4), 363–403, 1994.

553 Levitus, S., Antonov, J. I., Boyer, T. P., Baranova, O. K., Garcia, H. E., Locarnini, R. A., Mishonov, A. V., Reagan, J. R.,  
554 Seidov, D., Yarosh, E. S. and Zweng, M. M.: World ocean heat content and thermocline sea level change (0–2000 m),  
555 1955–2010. *Geophysical Research Letters* **39**(10). doi:10.1029/2012GL051106, 2012.

556 Lee S.-K., Park, W., Baringer, M. O., Gordon, A. L., Huber, B., and Liu, Y.: Pacific origin of the abrupt increase in Indian  
557 Ocean heat content. *Nature Geoscience*, **8**, 445-449, 2015.

558 Lee, T., and McPhaden, M. J.: Increasing intensity of El Niño in the central-equatorial Pacific. *Geophys. Res. Lett.*, **37**, L14603,  
559 doi:10.1029/2010GL044007, 2010.

560 Li, Z., Holbrook, N. J., Zhang, X., Oliver, E. C. J., and Coughon, E. A.: Remote Forcing of Tasman Sea Marine Heatwaves,  
561 *Journal of Climate*, **33**(12), 5337-5354, 2020.

562 Lorenzo, E. D., Mantua, N.: Multi-year persistence of the 2014/15 North Pacific marine heatwave, *Nature Cli. Change*, **6**,  
563 <https://www.nature.com/articles/nclimate3082>, 2016.

564 Mills, K. E., Andrew, J. P., Curtis, J. B., Yong, C., Fu-Sung, C., Daniel, S. H., Sigrid, L., Janet, A. N., Jenny, C.  
565 S., Andrew, C. T., Richard, A. W.: Fisheries management in a changing climate: lessons from the 2012 ocean heat wave  
566 in the Northwest Atlantic. *Oceanography* **26**, 191–195, 2013.

567 Montégut, de Boyer, C., Madec, G., Fischer, A. S., Lazar, A., and Iudicone, D. (2004), Mixed layer depth over the global  
568 ocean: An examination of profile data and a profile-based climatology, *J. Geophys. Res.*, **109**, C12003,  
569 doi:10.1029/2004JC002378.

570 Murakami, Hiroyuki, Delworth, T. L., Cooke, W. F., Zhao, M., Xiang, B. and Hsu, Pang-Chi: Detected climatic change in  
571 global distribution of tropical cyclones. *Proceedings of the National Academy of Sciences* **117**, 10706–10714, 2020.

572 Holbrook, N. J., Scannell, H. A., Gupta, A. S., Benthuisen, J. A., Feng, M., Oliver, E. C. J., Alexander, L. V., Burrows, M.  
573 T., Donat, M. G., Hobday, A. J., Moore, P. J., Perkins-Kirkpatrick, S. E., Smale, D. A.,  
574 Straub, S. C., Wernberg, T.: A global assessment of marine heatwaves and their drivers. *Nat. Commun.* **10**:2624, 2019.

575 Olita, A., Sorgente, R., Ribotti, A., Natale, S., and Gaberšek, S.: Effects of the 2003 European heatwave on the Central  
576 Mediterranean Sea surface layer: a numerical simulation. *Ocean Sci. Discuss*, 3, 85–125 (2006).

577 Oliver, E. C. J., Benthuisen, J. A., Bindoff, N. L., Hobday, A. J., Holbrook, N. J., Mundy, C. N., Perkins-Kirkpatrick, S. E.:  
578 The unprecedented 2015/16 Tasman Sea marine heatwave. *Nat. Commun.* 8:16101, 2017.

579 Oliver, E.: Mean warming not variability drives marine heatwave trends. *Climate Dynamics* 53 (3-4), pp. 1653-1659, 2019.  
580 doi: 10.1007/s00382-019-04707-2

581 Oliver, E. C. J., Benthuisen, J. A., Darmaraki, S., Donat, M. G., Hobday, A. J., Holbrook, N. J., Schlegel, R. W., Gupta, A.  
582 S.: Marine heatwaves, *Ann. Rev. Mar. Sci.*, 13, 313-342, <https://doi.org/10.1146/annurev-marine-032720-095144> , 2021.

583 Padmakumar, K. B., Menon, N. R., Sanjeevan, V. N.: Is Occurrence of Harmful Algal Blooms in the Exclusive Economic  
584 Zone of India on the Rise? *Int. J. of Ocean.*, 2012, 1-7, <https://doi.org/10.1155/2012/263946>, 2012.

585 Papa, F., Durand, F., Rossow, W. B., Rahman, A., and Bala, S. K.: Satellite altimeter-derived monthly discharge of the Ganga-  
586 Brahmaputra River and its seasonal to interannual variations from 1993 to 2008, *Journal of Geophysical Research*, 115,  
587 C12013, <https://doi.org/10.1029/2009JC006075>, 2010.

588 Pearce, A. F., Lenanton, R., Jackson, G., Moore, J., Feng, M., Gaughan, D.: The "marine heat wave" off Western Australia  
589 during the summer of 2010/11, *Tech. Rep. 222*, West. Aust. Fish. Mar. Res. Lab., North Beach,  
590 Australia, 2011.

591 Phillips, H. E., Tandon, A. et al.: Progress in understanding of Indian Ocean circulation, variability, air–sea exchange, and  
592 impacts on biogeochemistry, *Ocean Sci.*, 17, 1677-1751, 2021. <https://doi.org/10.5194/os-17-1677-2021>.

593 Praveen, K. B., Vialard, J., Lengaigne, M., Murty, V., and Mcphaden, M. J.: TropFlux: Air-sea fluxes for the global tropical  
594 oceans-description and evaluation. *Climate Dynamics*, 38(7-8), 1521–1543, 2012.

595 Praveen, K. B., Vialard, J., Lengaigne, M., Murty, V., Mcphaden, M. J., Cronin, M., Pinsard, F., Gopala, R. K.: TropFlux wind  
596 stresses over the tropical oceans: Evaluation and comparison with other products. *Climate Dynamics*, 40(7-8), 2049–2071,  
597 2013.

598 Rao, R. R. and Sivakumar, R.: On the possible mechanisms of the evolution of a mini-warm pool during the pre-summer  
599 monsoon season and the genesis of onset vortex in the southeastern Arabian Sea, *Quart. J. Roy. Met. Soc.*, 125, 787-  
600 809, 1999.

601 Reynolds, R. W., Smith, T. M., Liu, C., Chelton, D. B., Casey, K. S., and Schlax, M. G.: Daily high-resolution-blended analyses  
602 for sea surface temperature, *Journal of Climate*, 20(22), 5473–5496, <https://doi.org/10.1175/2007JCLI1824.1>, 2007.

603 Roxy, M., Ritika, K., Terray, P. and Masson, S.: The curious case of Indian Ocean warming, *J. Climate*, 27, 22, 8501-8509,  
604 2014.

605 Roxy, M., Ritika, K., Terray, P., Murtugudde, R., Ashok, K., Goswami, B. N.: Drying of Indian subcontinent by rapid Indian  
606 Ocean warming and a weakening land-sea thermal gradient. *Nat. Commun.*, 6, <https://doi.org/10.1038/ncomms8423>,  
607 2015.

608 Roxy, M. K., Modi, A., Murtugudde, R., Valsala, V., Panickal, S., Prasanna, K. S., Ravichandran, M., Vichi, M., and Lévy  
609 M.: A reduction in marine primary productivity driven by rapid warming over the tropical Indian Ocean, *Geophys. Res.*  
610 *Let.*, 43, 826–833, doi:10.1002/2015GL066979, 2016.

611 Roxy, M. K. , Gnanaseelan, C., Parekh, A., Chowdary, J. S., Singh, S., Modi, A., Kakatkar, R., Mohapatra, S.,  
612 and Dhara, C.: Indian Ocean warming, In *Assessment of Climate Change over the Indian Region*, Krishnan, R., Sanjay, J.,  
613 Gnanaseelan, C., Mujumdar, M., Kulkarni, A., Chakraborty, S., Eds., Springer, [https://doi.org/10.1007/978-981-15-4327-](https://doi.org/10.1007/978-981-15-4327-2)  
614 2, 2020.

615 Saji, N. H., Goswami, B. N., Vinayachandran, P. N. and Yamagata, T.: A dipole mode in the tropical Indian  
616 Ocean. *Nature*, **401**, 360–363. 1999.

617 Salinger MJ, Renwick J, Behrens E, Mullan AB, Diamond HJ, Sirguey, P., Smith, R. O., Trought, M. C. T., Alexander V, L.,  
618 Cullen, N. J.: The unprecedented coupled ocean-atmosphere summer heatwave in the New Zealand region 2017/18: drivers,  
619 mechanisms and impacts. *Environ. Res. Lett.*, 14:044023, 2019.

620 Saranya, J. S., Roxy, M. K., Dasgupta, P., and Anand, A.: Genesis and trends in marine heatwaves over the tropical Indian  
621 Ocean and their interaction with the Indian summer monsoon. *Journal of Geophysical Research: Oceans*, 127,  
622 e2021JC017427. <https://doi.org/10.1029/2021JC017427>, 2022.

623 Scannell, H. A., Pershing, A. J., Alexander, M. A., Thomas, A. C. and Mills, K. E.: Frequency of marine heatwaves in the  
624 North Atlantic and North Pacific since 1950, *Geophys. Res. Lett.*, 43, 2015GL067308, 2016.

625 Schott, F., and J. P. McCreary (2001), The monsoon circulation of the Indian Ocean, *Prog. Oceanogr.*, 51, 1–123.

626 Schlegel, R. W. and Smit, A. J.: heatwaveR: A central algorithm for the detection of heatwaves and cold-spells. *Journal of*  
627 *Open Source Software*, 3(27), 821, <https://doi.org/10.21105/joss.00821>, 2018.

628 Shankar D, Gopalakrishna VV, Shenoi SSC, Durand F, Shetye SR, Rajan CK, Johnson Z, Araligidad N, Michael G. S.:  
629 Observational evidence for westward propagation of temperature inversions in the southeastern Arabian Sea. *Geophys Res*  
630 *Lett*, 31, 2004. doi:10.1029-2004GL019652

631 Shankar, D., Remya, R., Vinayachandran, P., Chatterjee, A., and Behera, A.: Inhibition of mixed-layer deepening during winter  
632 in the northeastern Arabian Sea by the West India Coastal Current, *Climate Dynamics*, 47(3-4), 1049–1072, 2016.

633 Shankar, D., Remya, R., Anil, A. C., and Vijith, V.: Role of physical processes in determining the nature of fisheries in the  
634 eastern Arabian Sea, 172 (12), 10.1016/j.pocean.2018.11.006, 2018.

635 Shenoi, S. S. C., Shankar, D. and Shetye, S. R.: On the sea surface temperature high in the Lakshadweep Sea before the onset  
636 of southwest monsoon, *J. Geophys. Res.*, 104(C7), 15703 – 15712, 1999.

637 Sindhu, B., Suresh, I., Unnikrishnan, A., Bhatkar, N., Neetu, S., and Michael, G.: Improved bathymetric datasets for the  
638 shallow water regions in the Indian Ocean, *Journal of Earth System Science*, 116(3), 261–274, 2007.

639 Swapna, P., Krishnan, R. and Wallace, J.M.: Indian Ocean and monsoon coupled interactions in a warming environment. *Clim*  
640 *Dyn*, 42, 2439–2454, <https://doi.org/10.1007/s00382-013-1787-8>, 2014.

- 641 Trainer, V. L., Kudela, R. M., Hunter, M. V., Adams, N. G., and McCabe, R. M.: Climate Extreme Seeds a New Domoic Acid  
642 Hotspot on the US West Coast, *Front. Clim.*, 2:571836, doi: 10.3389/fclim.2020.571836, 2020.
- 643 Thomsen, M. S., Mondardini, L., Alestra, T., Gerrity, S., Tait, L., South, P. M., Lilley, S. A., Schiel, D. R.: Local extinction  
644 of bull kelp (*Durvillaea* spp.) due to a marine heatwave, *Front. Mar. Sci.* 6, 84, <https://doi.org/10.3389/fmars.2019.00084>,  
645 2019.
- 646 Vijith, V., Vinayachandran, P., Thushara, V., Amol, P., Shankar, D., and Anil, A.: Consequences of inhibition of mixed-layer  
647 deepening by the West India Coastal Current for winter phytoplankton bloom in the northeastern Arabian Sea, *Journal of*  
648 *Geophysical Research: Oceans*, 121, 6583–6603, <https://doi.org/10.1002/2016JC012004>, 2016.
- 649 Vinayachandran, P. N., and Shetye, S. R.: The warm pool in the Indian Ocean, *Proc. Indian Acad. Sci. (Earth Planet. Sci.)*,  
650 100(2), 165 – 175., 1991.
- 651 Vinayachandran, P. N., D. Shankar, J. Kurian, F. Durand, and S. S. C. Shenoi: Arabian Sea Mini Warm Pool and the Monsoon  
652 Onset Vortex. *Current Science* 93, no. 2 (2007): 203–14. <http://www.jstor.org/stable/24099306>.
- 653 Vinayachandran, P.N.M., Masumoto, Y., Roberts, M.J., Huggett, J.A., Halo, I., Chatterjee, A., Amol, P., Gupta, G.V., Singh,  
654 A., Mukherjee, A., Prakash, S., Beckley, L. E., Raes, E. J. and Hood, R.: Reviews and syntheses: Physical and  
655 biogeochemical processes associated with upwelling in the Indian Ocean. *Biogeosciences*, 18(22), pp.5967-6029, 2021.
- 656 Vörösmarty, C., Fekete, B., and Tucker, B.: River discharge database, Version 1.0 (RivDIS v1. 0), Volumes 0 through 6. A  
657 contribution to IHP-V Theme: 1. Technical documents in hydrology series. Paris: UNESCO, 1996.
- 658 Wernberg, T., Bennett, S., Babcock, R. C., De Bettignies, T., Cure, K., et al.: Climate- driven regime shift of a temperate  
659 marine ecosystem, *Science*, 353, 169–172, 2016.
- 660 Xie, S. P., Hu, K., Hafner, J., Tokinaga, H., Du, Y., Huang, G., and Sampe, T.: Indian Ocean capacitor effect on Indo-Western  
661 Pacific climate during the summer following El Nino. *J. Clim.* 22, 730-747, 2009.
- 662 Xie, T., Li, J., Chen, Chen, K., Zhang, Y., Sun, C.: Origin of Indian Ocean multidecadal climate variability: role of the North  
663 Atlantic Oscillation. *Clim Dyn*, 56, 3277–3294, <https://doi.org/10.1007/s00382-021-05643-w>, 2021.

664  
665  
666  
667  
668  
669  
670

671 **Figure 1:** Trend for the MHW days (days/year; left panels), MHW frequency (events/year; middle panels) and MHW intensity  
672 ( $^{\circ}\text{C}/\text{year}$ ; right panels) for the annual (a,b,c), pre-monsoon (d,e,f) and summer monsoon (g,h,i) periods. The trends within the  
673 99% confidence limit are marked by stippling. The black boxes represent the north Arabian Sea (NAS) and the southeastern  
674 Arabian Sea (SEAS). The trends are calculated for the period 1982-2019.

675 **Figure 2:** Boxplots representing the percentage of days experienced heatwaves during (a,d) annual, (b,e) pre-monsoon and  
676 (c,f) summer monsoon for the northern Arabian Sea (NAS) and the southeastern Arabian Sea (SEAS). The background shading  
677 represents the Niño3.4 index.

679 **Figure 3:** Maximum number of heatwave events observed each year across the northern Arabian Sea (top) and the southeastern  
680 Arabian Sea (SEAS).

682 **Figure 4:** Trends of SST ( $^{\circ}\text{C}/37$  years) over 1982-2019 for (a) annual, (b) pre-monsoon and (c) summer monsoon period.  
683 Stippling show regions where the trend is 99% significant based on two-tailed t-test.

685 **Figure 5:** Same as Figure 2, but using the detrended SST.

687 **Figure 6:** Ratio of MHW days derived using SST and detrended SST based on Equation (3).

689 **Figure 7:** (a) Correlation between MHW days based on detrended SST ( $^{\circ}\text{C}$ ) and major climate modes. Stippling represents  
690 regions where correlation is 99% significant. (b) Percentage of co-existing days between observed heatwaves and climate  
691 modes for annual, pre-monsoon and summer monsoon periods.

693 **Figure 8:** Evolution of observed SST (shading; daily averaged) with model simulated SST overlaid (contour) during April-  
694 June 2010. Regions experiencing MHWs are marked by stippling. The blue dot at the northcentral Arabian Sea ( $63^{\circ}\text{E}/19^{\circ}\text{N}$ )  
695 shows the location where the heat budget analysis was performed.

697 **Figure 9:** Same as Figure 8, but plotted daily to show the decaying phase of the heatwave event. The coloured curve on the  
698 panel for 2<sup>nd</sup> June 2010 represents track (and wind speed) of the tropical cyclone *Phet*.

700 **Figure 10:** Event line plot of the 2010 pre-monsoon heatwave event at the northcentral Arabian Sea ( $63^{\circ}\text{E}/19^{\circ}\text{N}$ ). The red  
701 shading marks the departure of observed SST from the threshold i.e., the heatwave event. The blue line is the model simulated  
702 SST. The green dashed line marks the initiation date of the tropical cyclone *Phet*.

704 **Figure 11:** Mixed layer heat budget analysis at the northcentral Arabian Sea ( $63^{\circ}\text{E}/19^{\circ}\text{N}$ ). The "sum of terms" represents the  
705 sum of all terms on the right side of Equation (1).

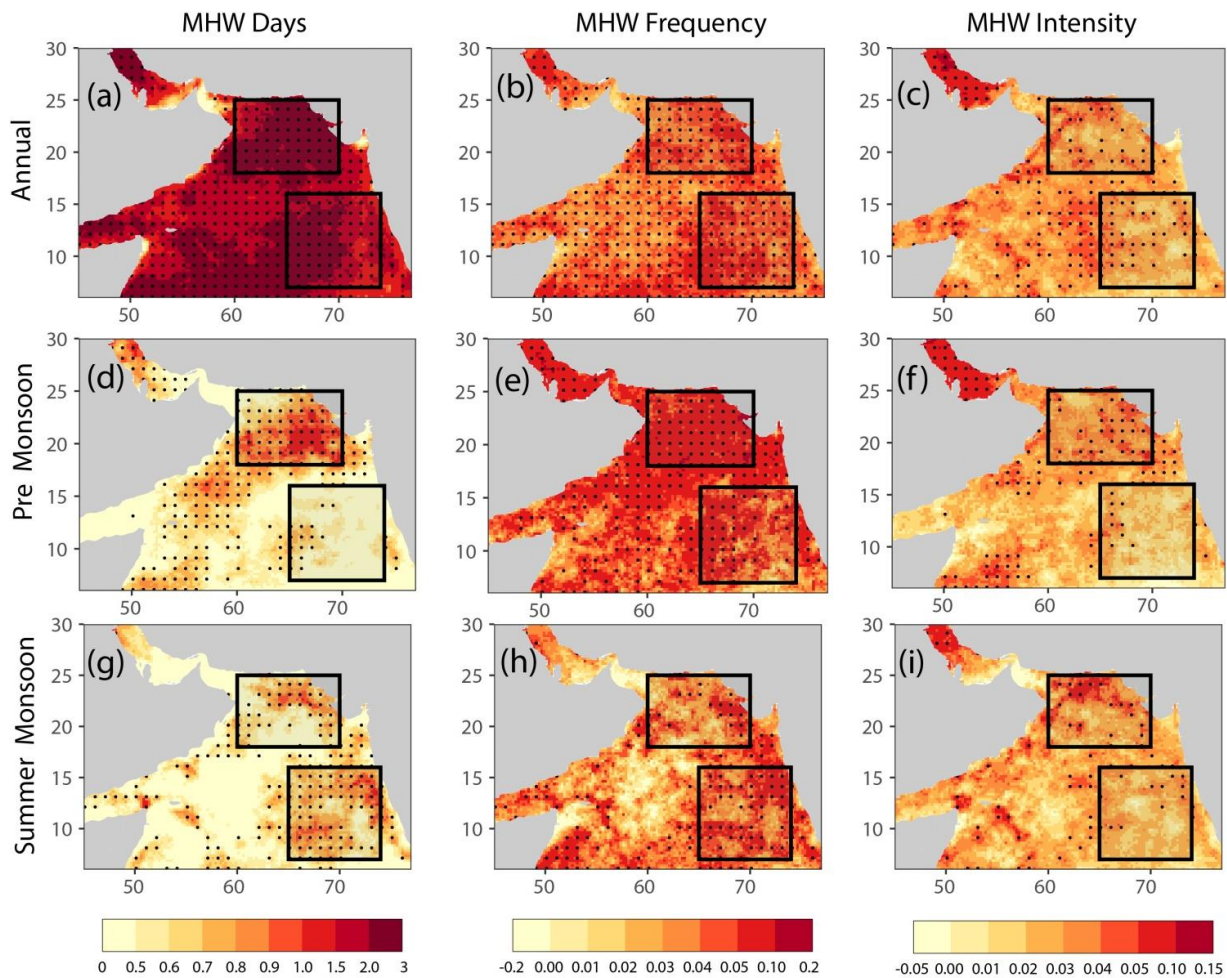
707 **Figure 12:** Model simulated mixed layer depth (top) and anomaly (bottom) for March-June 2010.

709 **Figure 13:** Surface heat fluxes, wind speed and mixed layer depth at the northcentral Arabian Sea during March-June 2010.

711 **Figure 14:** Cyclone tracks and their wind speeds during 2000-2010 (left) and 2011-2022. The cyclone Nisagra is marked by  
712 its propagation dates.

714 **Figure 15:** Event line during March-July 2020 at a location off the west coast of India (off Goa). The green dashed line  
715 represents the date when the Nisagra cyclone passed over off Goa, India.

716



717

718

**Figure 1:** Trend for the MHW days (days/year; left panels), MHW frequency (events/year; middle panels) and MHW intensity

719

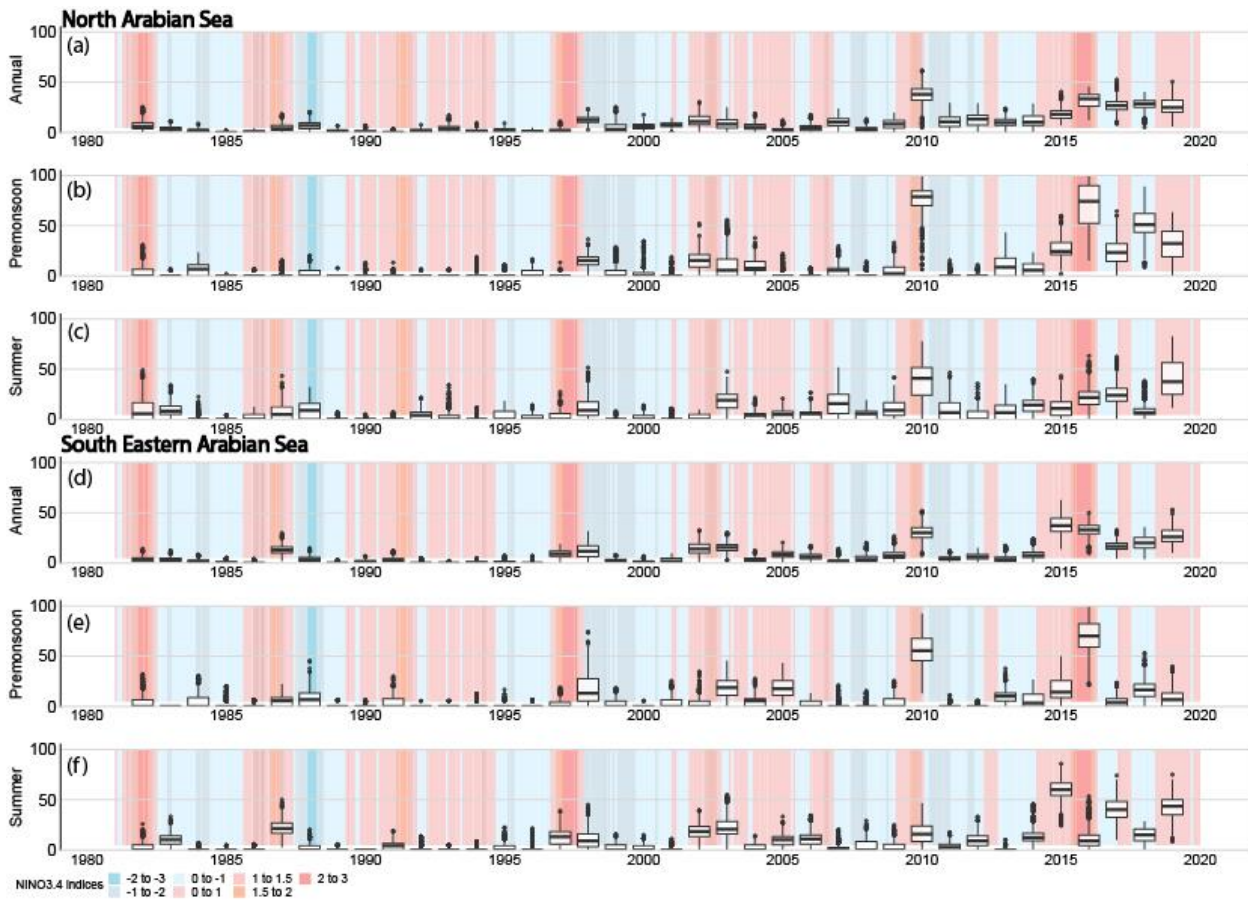
(°C/year; right panels) for the annual (a,b,c), pre-monsoon (d,e,f) and summer monsoon (g,h,i) periods. The trends within the

720

99% confidence limit are marked by stippling. The black boxes represent the north Arabian Sea (NAS) and the southeastern

721

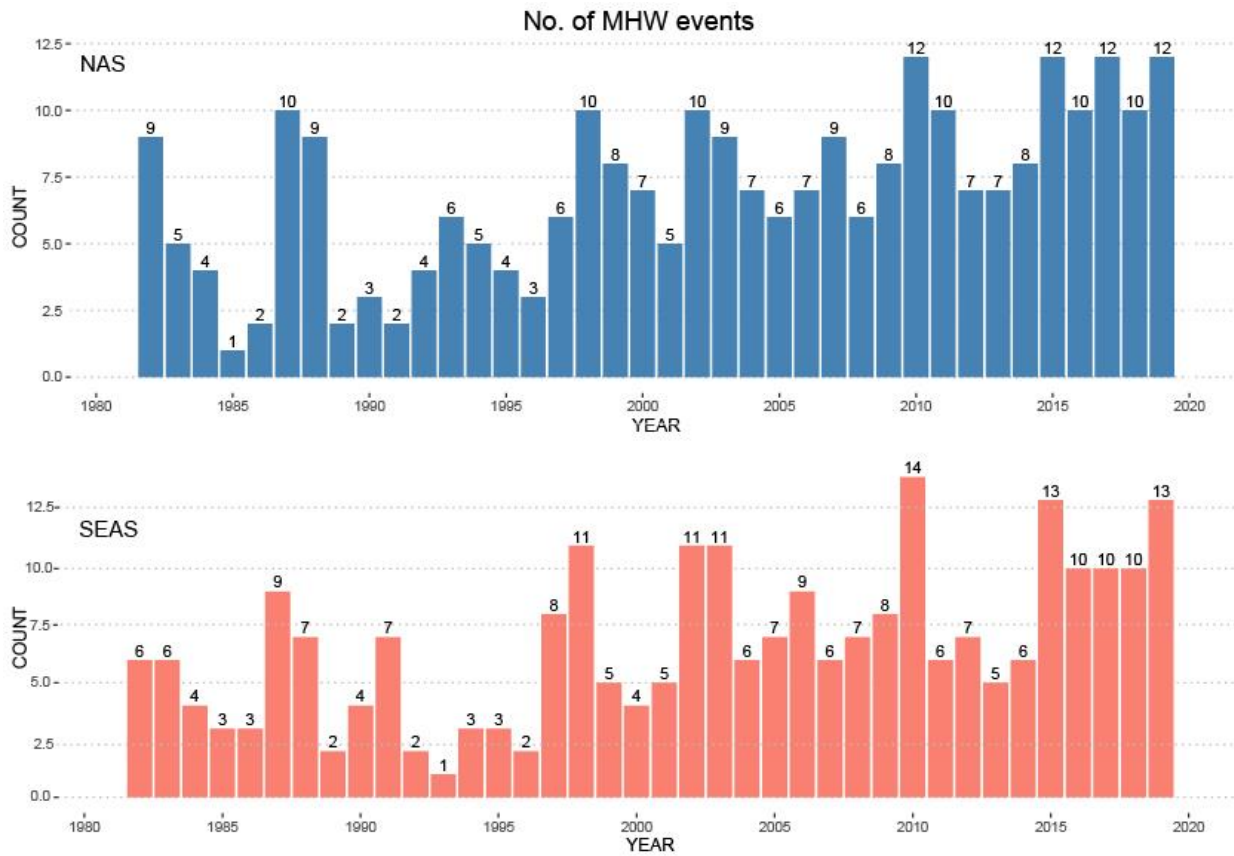
Arabian Sea (SEAS). The trends are calculated for the period 1982-2019.



722  
723  
724  
725

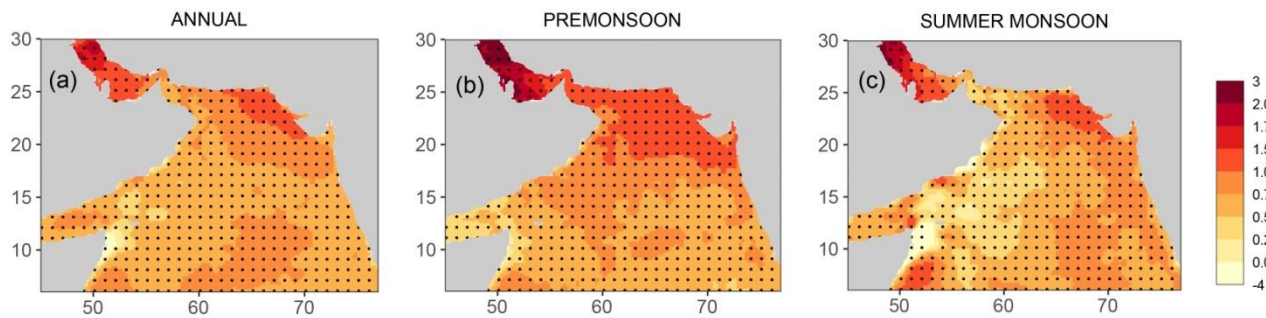
**Figure 2:** Boxplots representing the percentage of days experienced heatwaves during (a,d) annual, (b,e) pre-monsoon and (c,f) summer monsoon for the northern Arabian Sea (NAS) and the southeastern Arabian Sea (SEAS). The background shading represents the Niño3.4 index.





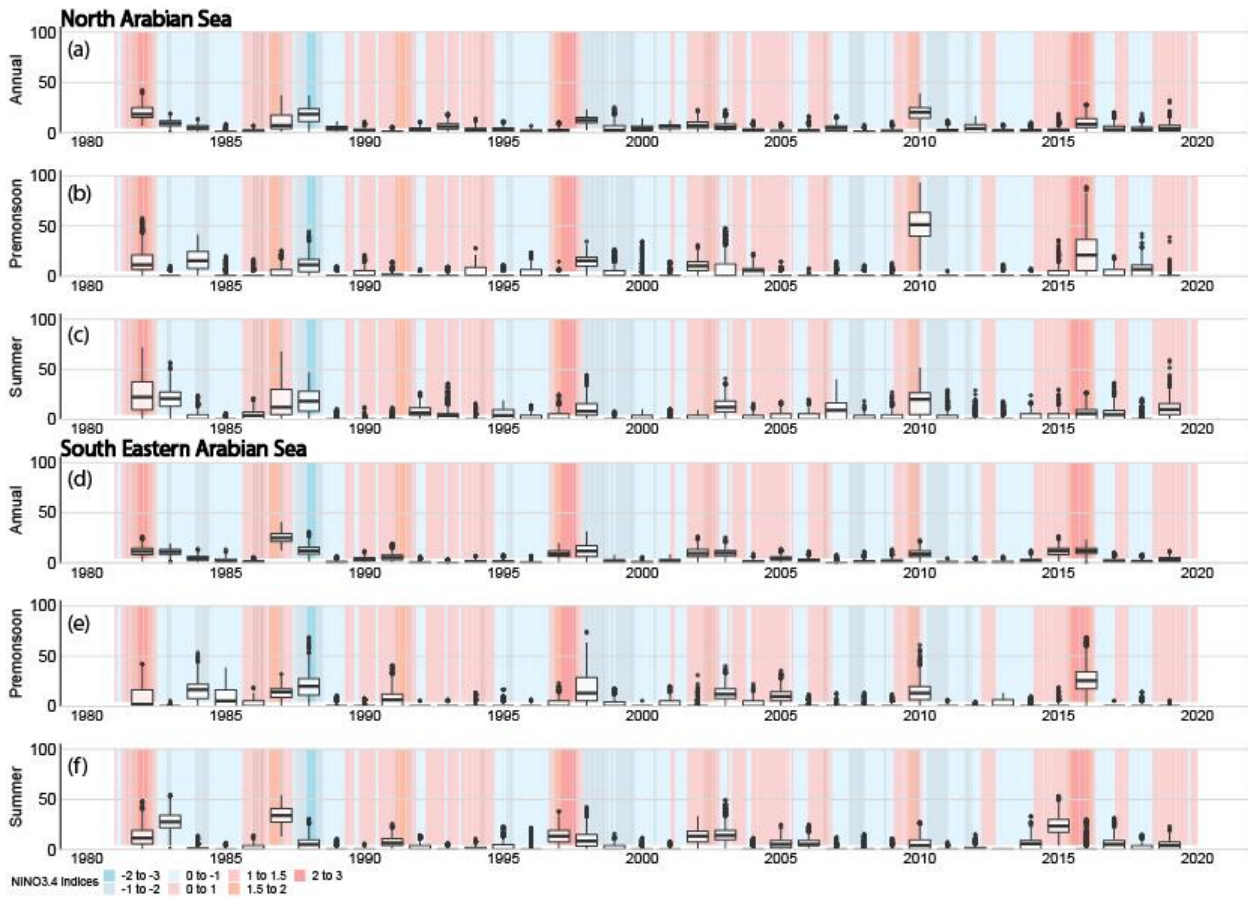
726  
727  
728  
729

**Figure 3:** Maximum number of heatwave events observed each year across the northern Arabian Sea (top) and the southeastern Arabian Sea (SEAS).

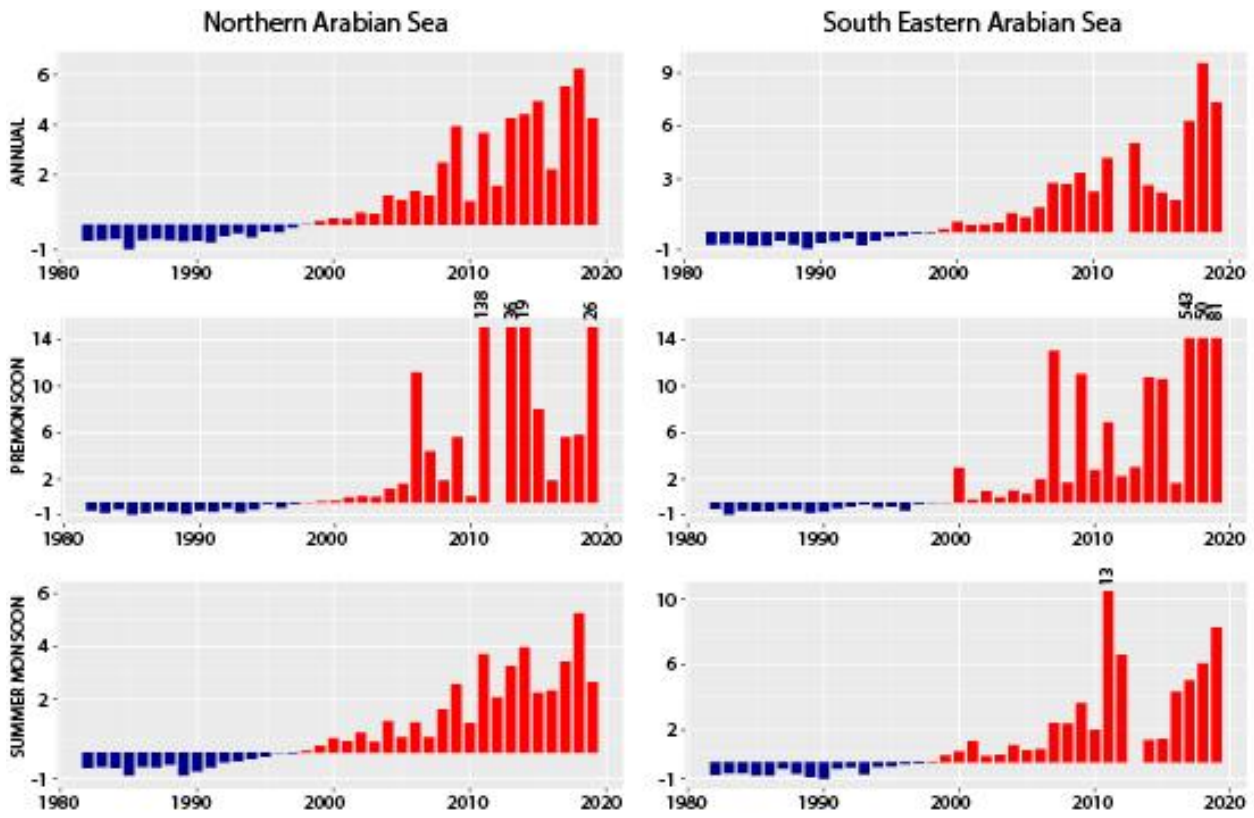


730  
731  
732

**Figure 4:** Trends of SST ( $^{\circ}\text{C}/37$  years) over 1982-2019 for (a) annual, (b) pre-monsoon and (c) summer monsoon period. Stippling show regions where the trend is 99% significant based on two-tailed t-test.

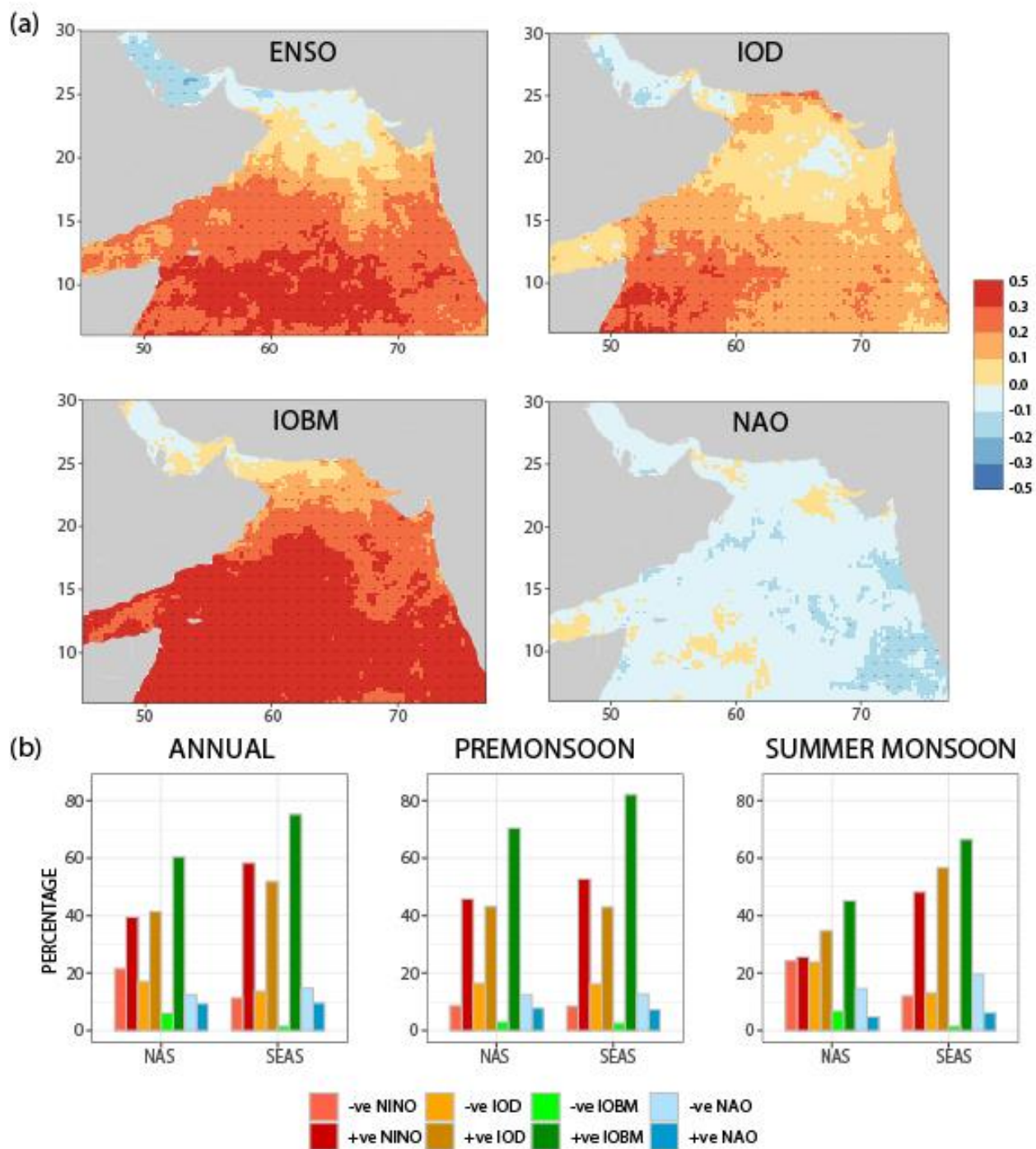


733  
734 **Figure 5:** Same as Figure 2, but using the detrended SST.

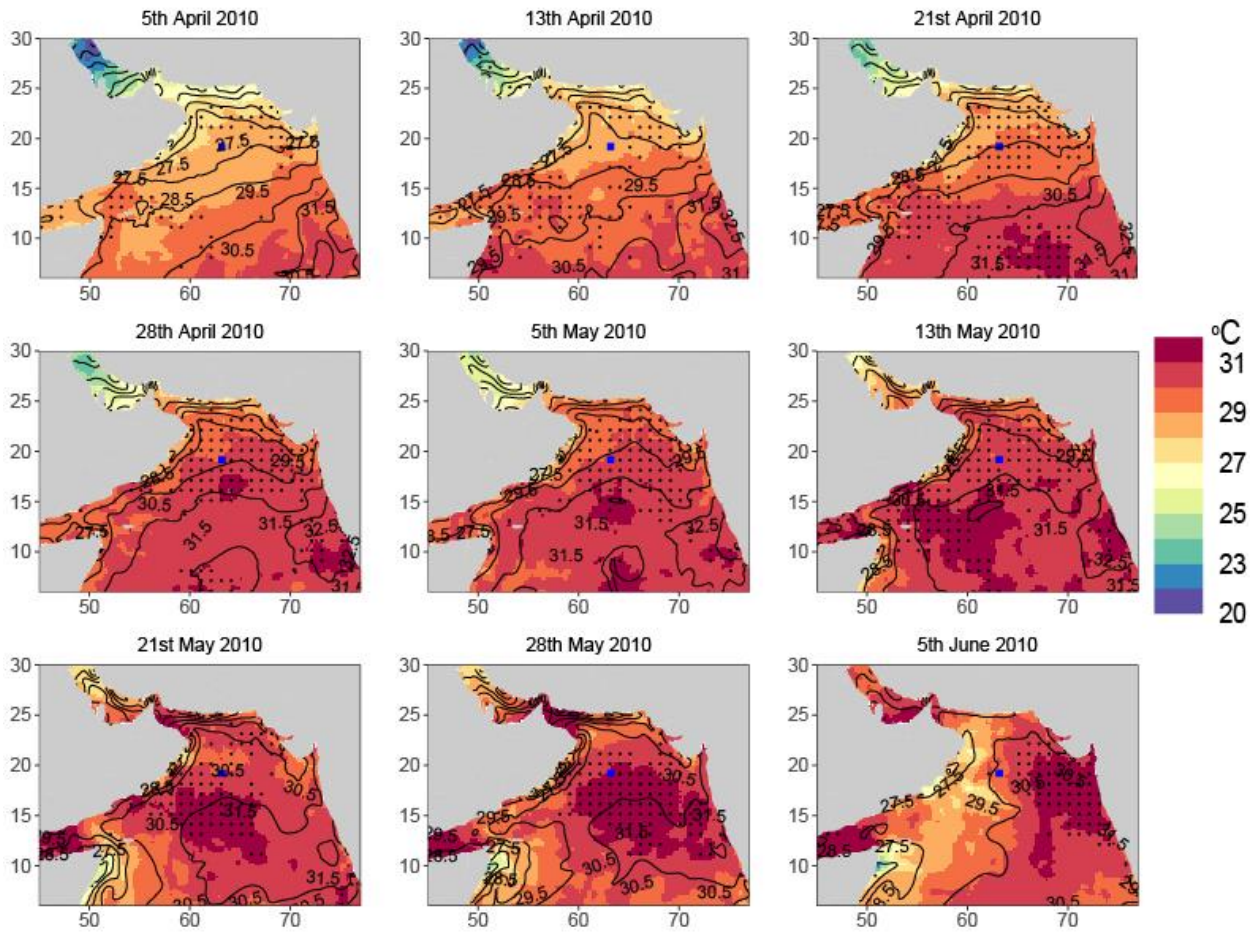


735  
736

**Figure 6:** Ratio of MHW days derived using SST and detrended SST based on Equation (3).

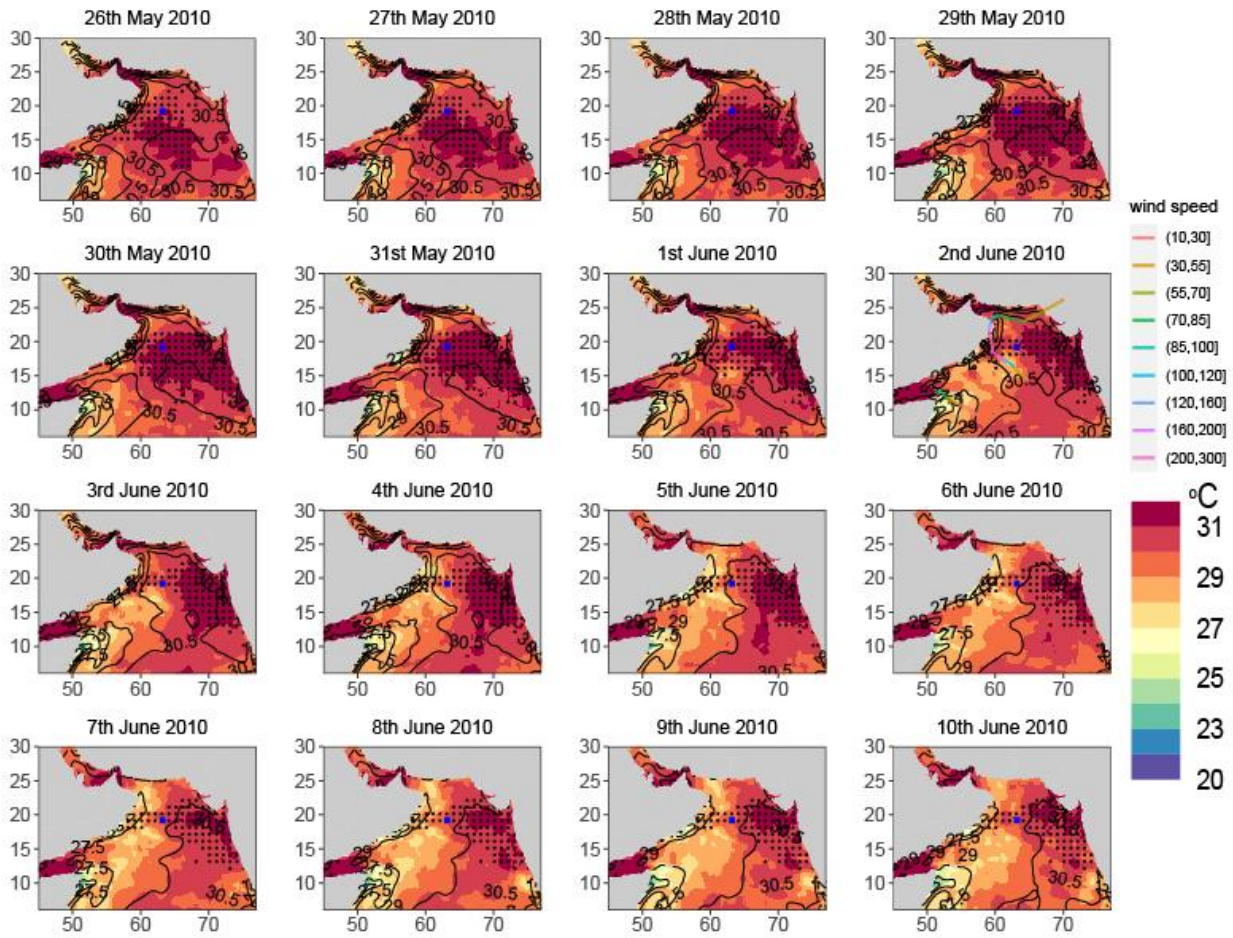


737  
 738 **Figure 7:** (a) Correlation between MHW days based on detrended SST ( $^{\circ}$ C) and major climate modes. Stippling represents  
 739 regions where correlation is 99% significant. (b) Percentage of co-existing days between observed heatwaves and climate  
 740 modes for annual, pre-monsoon and summer monsoon periods.



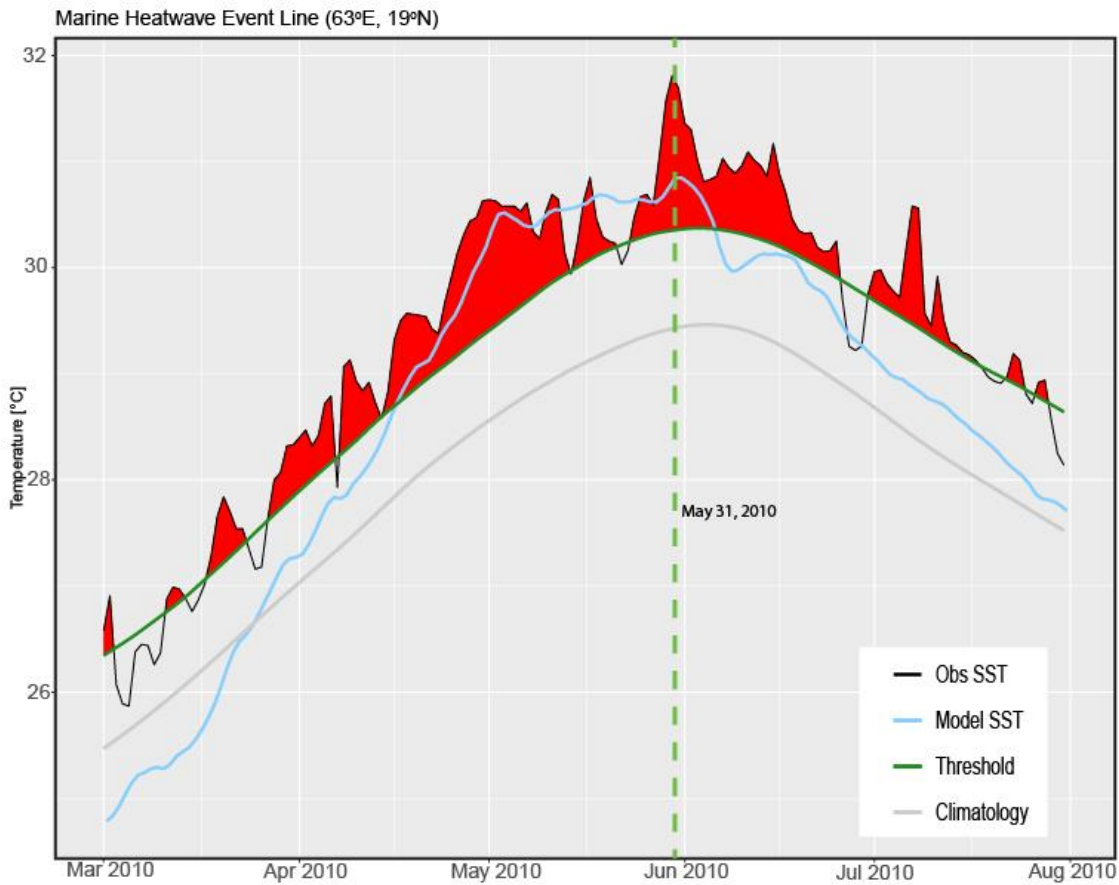
741  
742  
743  
744  
745

**Figure 8:** Evolution of observed SST (shading; daily averaged) with model simulated SST overlaid (contour) during April-June 2010. Regions experiencing MHWs are marked by stippling. The blue dot at the northcentral Arabian Sea (63°E/19°N) shows the location where the heat budget analysis was performed. Note that SST maps are daily averaged fields for the particular day of the year 2010.



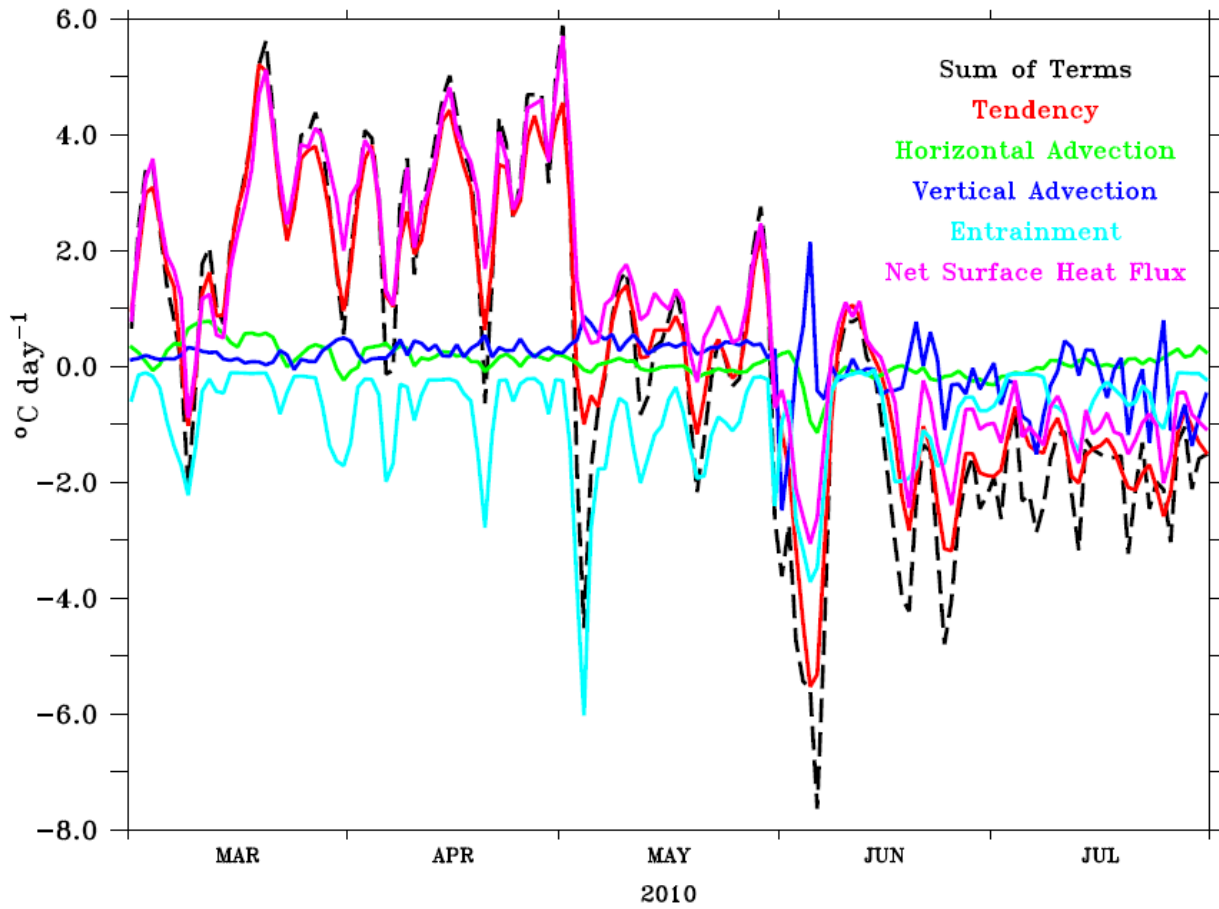
746  
747  
748

**Figure 9:** Same as Figure 8, but plotted daily to show the decaying phase of the heatwave event. The coloured curve on the panel for 2<sup>nd</sup> June 2010 represents track (and wind speed) of the tropical cyclone *Phet*.



749  
750  
751  
752  
753

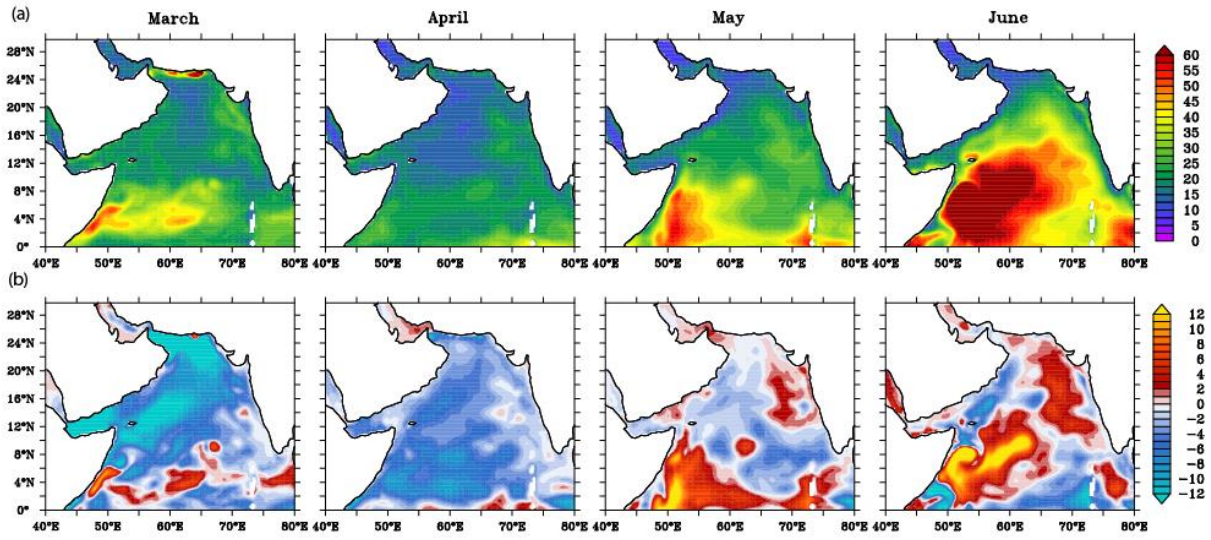
**Figure 10:** Event line plot of the 2010 pre-monsoon heatwave event at the northcentral Arabian Sea (63°E/19°N). The red shading marks the departure of observed SST from the threshold i.e., the heatwave event. The blue line is the model simulated SST. The green dashed line marks the initiation date of the tropical cyclone *Phet*.



754  
755  
756  
757

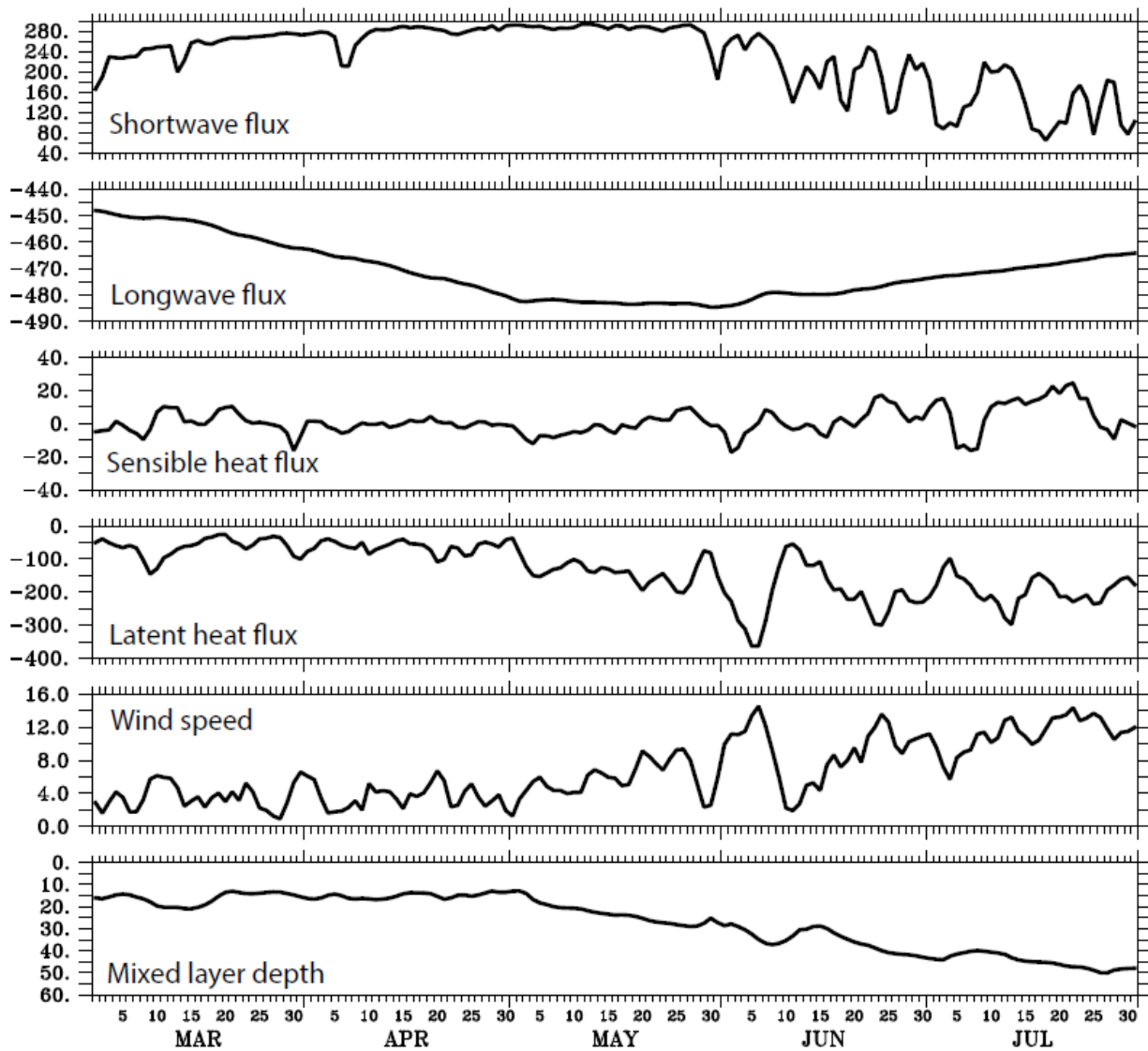
**Figure 11:** Mixed layer heat budget analysis at the northcentral Arabian Sea (63°E/19°N). The "sum of terms" represents the sum of all terms on the right side of Equation (1).



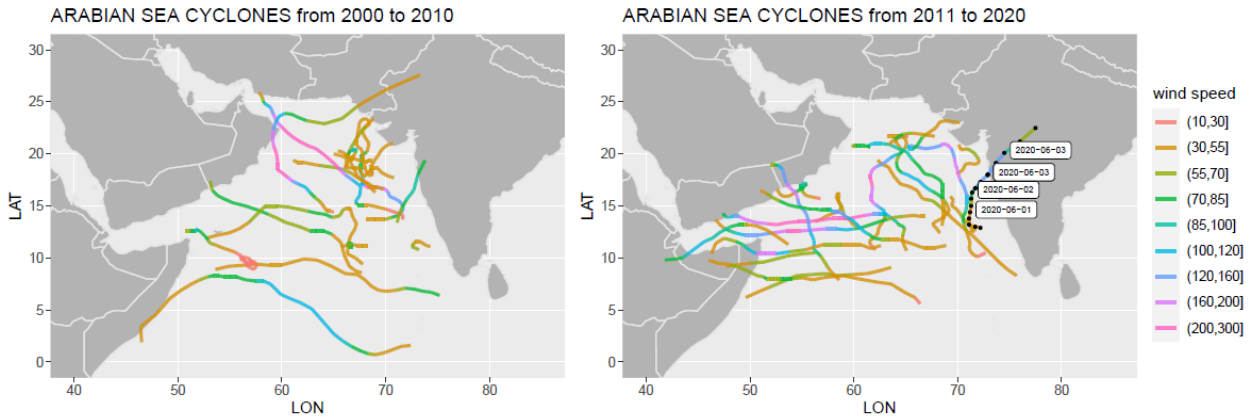


758  
759

**Figure 12:** Model simulated mixed layer depth (top) and anomaly (bottom) for March-June 2010.

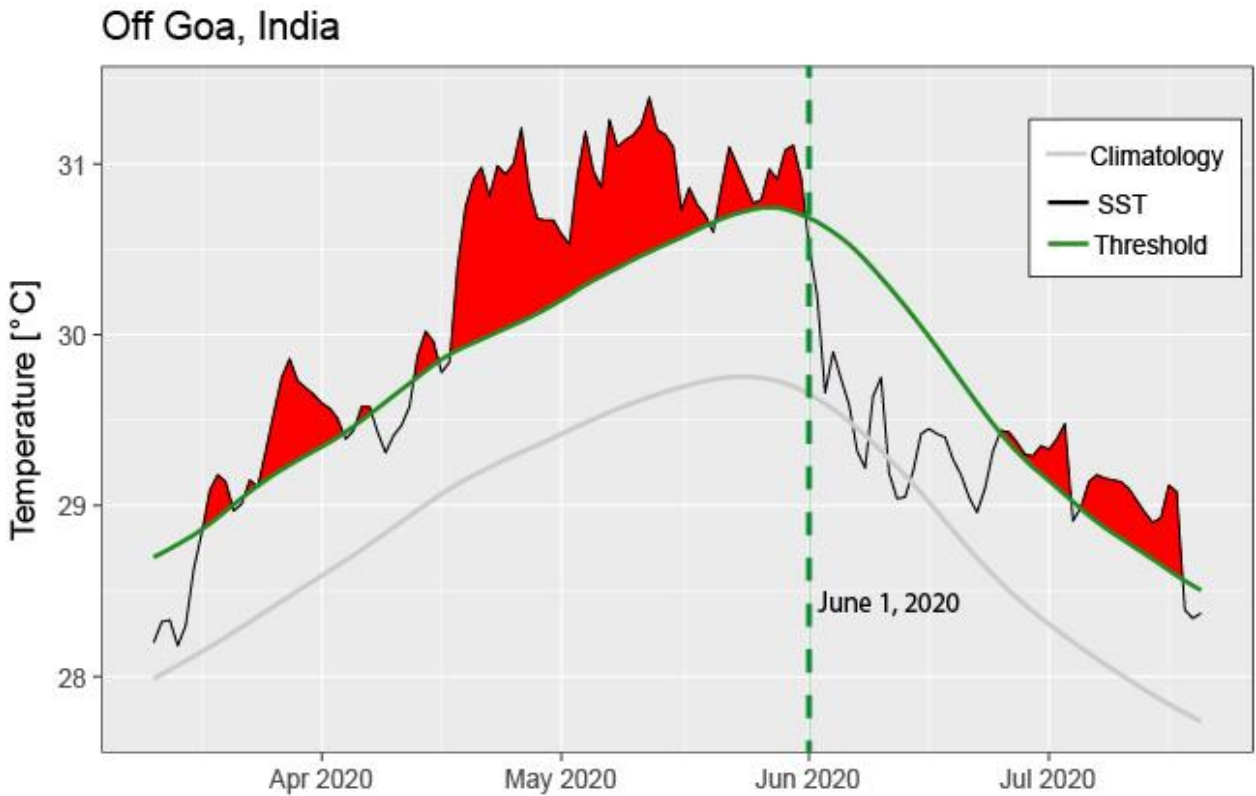


760 **Figure 13:** Surface heat fluxes, wind speed and mixed layer depth at the northcentral Arabian Sea during March-June 2010.  
 761  
 762



763  
764  
765

**Figure 14:** Cyclone tracks and their wind speeds during 2000-2010 (left) and 2011-2022. The cyclone track of Nisagra is marked by its propagation dates.



766  
767  
768  
769

**Figure 15:** Event line during March-July 2020 at a location off the west coast of India (off Goa). The green dashed line represents the date when the Nisagra cyclone passed over off Goa, India.